Systems/Circuits

Shaping the Output of Lumbar Flexor Motoneurons by Sacral Neuronal Networks

Meir Cherniak, Lili Anglister, and Aharon Lev-Tov

Department of Medical Neuroscience, Institute for Medical Research, Israel–Canada, the Hebrew University-Hadassah Medical School, Jerusalem, 9112102 Israel

The ability to improve motor function in spinal cord injury patients by reactivating spinal central pattern generators (CPGs) requires the elucidation of neurons and pathways involved in activation and modulation of spinal networks in accessible experimental models. Previously we reported on adrenoceptor-dependent sacral control of lumbar flexor motoneuron firing in newborn rats. The current work focuses on clarification of the circuitry and connectivity involved in this unique modulation and its potential use. Using surgical manipulations of the spinal gray and white matter, electrophysiological recordings, and confocal microscopy mapping, we found that methoxamine (METH) activation of sacral networks within the ventral aspect of S2 segments was sufficient to produce alternating rhythmic bursting (0.15–1 Hz) in lumbar flexor motoneurons. This lumbar rhythm depended on continuity of the ventral funiculus (VF) along the S2–L2 segments. Interrupting the VF abolished the rhythm and replaced it by slow unstable bursting. Calcium imaging of S1–S2 neurons, back-labeled via the VF, revealed that ~40% responded to METH, mostly by rhythmic firing. All uncrossed projecting METH responders and ~70% of crossed projecting METH responders fired with the concurrent ipsilateral motor output, while the rest (~30%) fired with the contralateral motor output. We suggest that METH-activated sacral CPGs excite ventral clusters of sacral VF neurons to deliver the ascending drive required for direct rhythmic activation of lumbar flexor motoneurons. The capacity of noradrenergic-activated sacral CPGs to modulate the activity of lumbar networks via sacral VF neurons provides a novel way to recruit rostral lumbar motoneurons and modulate the output required to execute various motor behaviors.

Key words: **adrenoceptors; ascending pathways; calcium imaging; central pattern generators; sacrocaudal afferents; spinal interneurons**

Significance Statement

Spinal central pattern generators (CPGs) produce the rhythmic output required for coordinating stepping and stabilizing the body axis during movements. Electrical stimulation and exogenous drugs can reactivate the spinal CPGs and improve the motor function in the absence of descending supraspinal control. Since the body-stabilizing sacral networks can activate and modulate the limb-moving lumbar circuitry, it is important to clarify the functional organization of sacral and lumbar networks and their linking pathways. Here we decipher the ascending circuitry linking adrenoceptor-activated sacral CPGs and lumbar flexor motoneurons, thereby providing novel insights into mechanisms by which sacral circuitry recruits lumbar flexors, and enhances the motor output during lumbar afferent-induced locomotor rhythms. Moreover, our findings might help to improve drug/electrical stimulation-based therapy to accelerate locomotor-based rehabilitation.

Introduction

Spinal central pattern generators (CPGs) modulated by descending supraspinal commands produce the coordinated rhythmic patterns that mammals need for stepping (for review, see Alford et al., 2003; Kiehn, 2006; Hultborn and Nielsen, 2007; Frigon, 2012). When the descending connectivity is impaired, the CPGs can be reactivated by afferent inputs (Grillner and Rossignol, 1978; Grillner and Zangger, 1979; Pearson and Rossignol, 1991; Leblond et al., 2003; Wernig et al., 1998; Dietz et al., 2002; for review, see Pearson, 2004; Majczyński and Sławińska, 2007; Rossignol and Frigon, 2011; Edgerton et al., 2008; Hubli and Dietz, 2013). The ability of reactivated CPGs in spinal cord injury pa-

Received July 12, 2016; revised Dec. 11, 2016; accepted Dec. 14, 2016.

Author contributions: L.A. and A.L.-T. designed research; M.C. performed research; M.C. and A.L.-T. analyzed data; L.A. and A.L.-T. wrote the paper.

This work was supported by the Israel Science Foundation (Grants 1591/08, 1930/08, 491/12, and 1833/16 to A.L.-T). We thank Drs. M. J. O'Donovan and I. Silman for their valuable comments on the manuscript.

The authors declare no competing financial interests.

Correspondence should be addressed to either Aharon Lev-Tov, PhD, or Lili Anglister, PhD, Department of Medical Neurobiology, The Hebrew University Medical School, Jerusalem, 9112102 Israel, E-mail: aharonl@ekmd.huji.ac.il or lili.anglister@huji.ac.il.

DOI:10.1523/JNEUROSCI.2213-16.2016

 0270-6474/17/371294-18$15.00/0

tients to improve motor function (Hubli and Dietz, 2013) makes it especially important to elucidate in accessible experimental models the networks and pathways involved in activation and modulation of CPGs.

The *in vitro* spinal cord preparation of newborn rodents (Kudo and Yamada, 1987; Smith et al., 1988) is an ideal model for studying functional organization and mechanism of action of mammalian CPGs in the absence of supraspinal control. Studies of spinal cords of newborn rodents revealed that lumbar hindlimb-moving CPGs can be activated neurochemically mainly by bath-applied NMDA/5HT (for review, see Kiehn, 2006; Miles and Sillar, 2011). These CPGs are also activated by stimulation of sacrocaudal afferents (SCAs; Lev-Tov et al., 2000; Whelan et al., 2000; Strauss and Lev-Tov, 2003; Mandadi and Whelan, 2009; Cherniak et al., 2014; Klein and Tresch, 2010) and lumbar afferents (Marchetti et al., 2001; Taccola, 2011; Dose et al., 2016).

Sacrocaudal CPGs (SCPGs) which control the axial and tail musculature and assure body stabilization during various behaviors have received much less attention than the locomotor CPGs (LCPGs). However, sacral networks were shown to play a major role in SCA-dependent activation of LCPGs (Strauss and Lev-Tov, 2003; Blivis et al., 2007; Etlin et al., 2010, 2013; Lev-Tov et al., 2010; Cherniak et al., 2014).

Neurochemical activation of SCPGs also modulates the output of lumbar motoneurons. We reported that the α1-adrenoceptor agonist methoxamine (METH) is an effective activator of SCPGs. METH produces in sacral motoneurons and lumbar flexor motoneurons long-lasting 0.25–1 Hz rhythm that persists in detached SC segments (Gabbay and Lev-Tov, 2004). Another α1-adrenoceptor agonist, phenylephrine, was found to increase the amplitude and duration of SCA-induced rhythm in newborn mice (Gordon and Whelan, 2006). Noradrenaline, a known modulator of CPGs (for review, see Miles and Sillar, 2011), was found to be less effective than METH in neonatal rat spinal cords. It produced in sacral and lumbar motoneurons a "fast" rhythm that quickly transformed into the typical slow non-locomotor rhythm previously described (Kiehn et al., 1999; Cazalets and Bertrand, 2000; Sqalli-Houssaini and Cazalets, 2000). The classical activator of LCPGs, NMDA/5HT, was also ineffective: it failed to activate the SCPGs in detached sacrocaudal segments (Gabbay et al., 2002).

Therefore, the METH-activated sacral circuitry provides a potent means to regulate the output of lumbar flexor motoneurons in rats. The circuitry and pathways involved in this unique adrenoceptor-dependent sacral control of lumbar flexor motoneuron output are unknown, and the current work focuses on their elucidation and potential use.

Using surgical and pharmacological manipulations, we found that the circuitry in the ventral aspect of the second sacral segment (S2) was sufficient to produce the "fast" METH rhythm in sacral and lumbar flexor motoneurons. Moreover, sacral METH enhanced the hindlimb locomotor rhythm produced by lumbar afferent stimulation. We provide evidence that sacral relay interneurons with direct projections to rostral lumbar segments deliver the drive produced by METH-activated SCPGs to the lumbar cord, exclusively through the ventral funiculus (VF). Calcium imaging of sacral VF neurons (VFNs) revealed that they discharged rhythmically during METH activation of the SCPGs to elicit rhythmic bursting in their target lumbar flexor motoneurons.

Thus, the capacity of the noradrenergic-activated SCPGs to modulate the activity of lumbar networks via sacral VFNs provides a novel way to recruit lumbar flexor motoneurons and modulate the motor output required to execute various motor behaviors.

Materials and Methods

Materials. All chemicals, buffers, and reagents were of analytical grade. The drugs used in this work were the non-NMDA receptor blocker CNQX, the NMDA receptor blocker APV, and the α1-adrenoceptor agonist METH. All products were purchased from Sigma-Aldrich unless specified otherwise.

Animals and preparations. All procedures were approved by The Hebrew University Ethics Committee and performed according to its guidelines. The Hebrew University is accredited by the Association for Assessment and Accreditation of Laboratory Animal Care. The experiments were performed on newborn Sprague Dawley rats received from the university's official supplier (Harlan Laboratories) on the day of the experiment. Spinal cords (T6-Co3) were isolated from postnatal day (P) 1–P3 isoflurane-anesthetized male or female rats (Lev-Tov and Delvolvé, 2000; Lev-Tov et al., 2000; Delvolvé et al., 2001; Blivis et al., 2007). Preparations were transferred to a recording chamber and superfused continuously with oxygenated artificial CSF (ACSF; Kremer and Lev-Tov, 1997; Lev-Tov et al., 2000; Delvolvé et al., 2001; Blivis et al., 2007).

Surgical manipulations. Surgical manipulations of spinal cord preparations were done to determine the contribution of sacral networks to the origination of lumbar METH rhythm. Ultrafine clipper scissors with 75-μm-thick blades (Fine Science Tools; Etlin et al., 2010) were used to remove specific sacral segments, lesion the dorsal aspect of the cord, or interrupt the white matter funiculi, as specified in the respective parts of Results. Preparations were washed with ACSF for $\geq$45 min before attempting to re-elicit rhythmic activity.

The microscopic location and extent of the lesions were confirmed by histological examination of 20-μm-thick cross sections of paraffin-embedded preparations (Etlin et al., 2010; see Fig. 6*A*,*B*), or of 100–200 μm vibratome sections of the fixed preparations (see Fig. 3*A*,*B*), after completion of the electrophysiological recordings.

Stimulation and recordings. Suction electrode recordings were obtained from pairs of lumbar and sacral ventral roots using a 0.1 Hz to 10 kHz AC amplifier (Fig. 1).

Rhythmic activity. Rhythmic activity was induced by bath application of the α1-adrenoceptor agonist METH (50–100 μM) or, when required, by graded electrical stimulation of SCAs, traveling mainly through the first or second coccygeal dorsal roots (Co1-Co2; see Fig. 9). The threshold was measured from the polysynaptic response produced by single-pulse stimulation in the ipsilaterally recorded sacral and lumbar ventral roots (Etlin et al., 2010). When required, the experimental bath was divided into two or three compartments by Vaseline barrier(s) to test regionally dependent effects of various drugs (Figs. 1*C*, 2*A*, 6*D*).

Fluorescent labeling and confocal microscopy. Sacral VF neurons were labeled by loading fluorescein dextran (Invitrogen) into axon bundles peeled away from the VF (Fig. 3) at the lumbosacral junction and drawn into a suction electrode containing ~20% w/v of the dye dissolved in distilled water with or without 0.2% Triton X-100 for ~15 h (O'Donovan et al., 1993; Etlin et al., 2010, 2013; Finkel et al., 2014). Isolated spinal cords were then fixed in 4% paraformaldehyde (in PBS) for 4–10 h at 4°C, subsequently embedded in warm 5% agar (in PBS), and 50–100 μm sections were cut with a vibratome. The sections were mounted in fluorescence antifade mounting medium (Dako North America) and processed for morphological analysis (Etlin et al., 2010, 2013; Mor et al., 2012a,b; Finkel et al., 2014). When required (Fig. 3), images were obtained using a confocal microscope (Fluoview 1000, Olympus) equipped with three single-photon lasers. The spinal sections were scanned and photographed at 10× magnification to view the whole spinal segment.

Imaging of sacral VF neuron activity with calcium-sensitive dyes. Details about retrograde labeling with calcium fluorescent indicators and the visualization techniques have been previously reported (O'Donovan et al., 1993, 1994; Lev-Tov and O'Donovan, 1995; Bonnot et al., 2002, 2005; Etlin et al., 2013). Briefly, sacral VF neurons were retrogradely labeled by soaking narrow strips of cut VF axon bundles at the lumbosacral junction with 25–50 mM Calcium Green dextran (Invitrogen) applied through a tightly fitting suction electrode. Following 12–16 h of loading, the cord

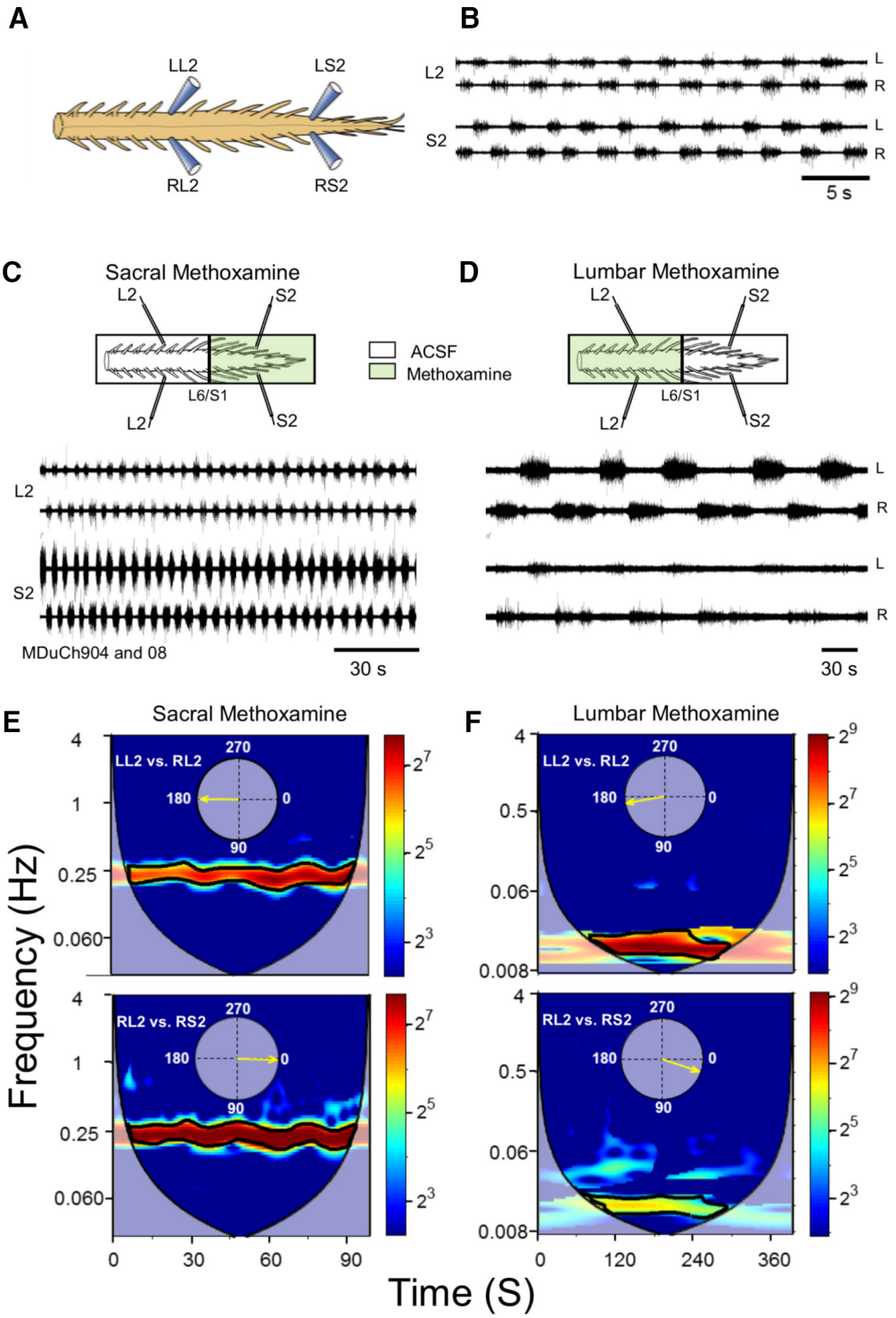

Figure 1. The 0.15–1 Hz lumbar METH rhythm originates from activated sacral neuronal networks. ***A***, Schematic view of the isolated spinal cord preparation and the recordings made from the left and right ventral roots of the second lumbar (L2) and sacral (S2) ventral roots. ***B***, Recordings (AC, 20 Hz to 10 kHz) from the left (L) and right (R) ventral roots of S2 and L2 in the presence of 50 μM METH. ***C***, ***D***, AC recordings (20 Hz to 10 kHz) from the left (L) and right (R) ventral roots of the S2 and L2, 10 min after addition of 100 μM METH to the sacral compartment of a dual-chamber experimental bath (***C***, Sacral Methoxamine), and 10 min after addition of METH to the lumbar compartment (***D***, Lumbar Methoxamine). Lumbar application of METH followed 45 min of washing the METH out of the sacral chamber. ***E***, ***F***, Coherent cross-power density plots of the activity recorded following sacral (***E***) and lumbar (***F***) application of METH show high-power (color-coded) frequency bands (heavy black lines) of the left L2 (LL2) versus right L2 (RL2) and RL2 versus RS2 time series shown in ***C*** and ***D***. The mean ± SEM values of the frequency and power, and the mean phase shifts and r-vectors (insets) were extracted from 10 consecutive epochs of the respective high-power frequency bands of the spectra in ***E*** and ***F***. Details of the statistical analyses and significant differences are described in Materials and Methods, Data acquisition and analyses.

was mounted in a chamber equipped for electrophysiological recording and viewed, using epifluorescence microscopy (BX51WI, Olympus), at the caudal S1 and the entire S2 segment through the ventral aspect of the cord. Images were made with a cooled 14-bit CCD camera (EXI Aqua, QImaging). These methods were sufficient to visualize and image sacral VF neurons residing within the ventral gray matter close to the ventral surface of the spinal cord (Etlin et al., 2013). Labeled VFNs were visualized using a water-immersion 20× objective (numerical aperture, 0.5),

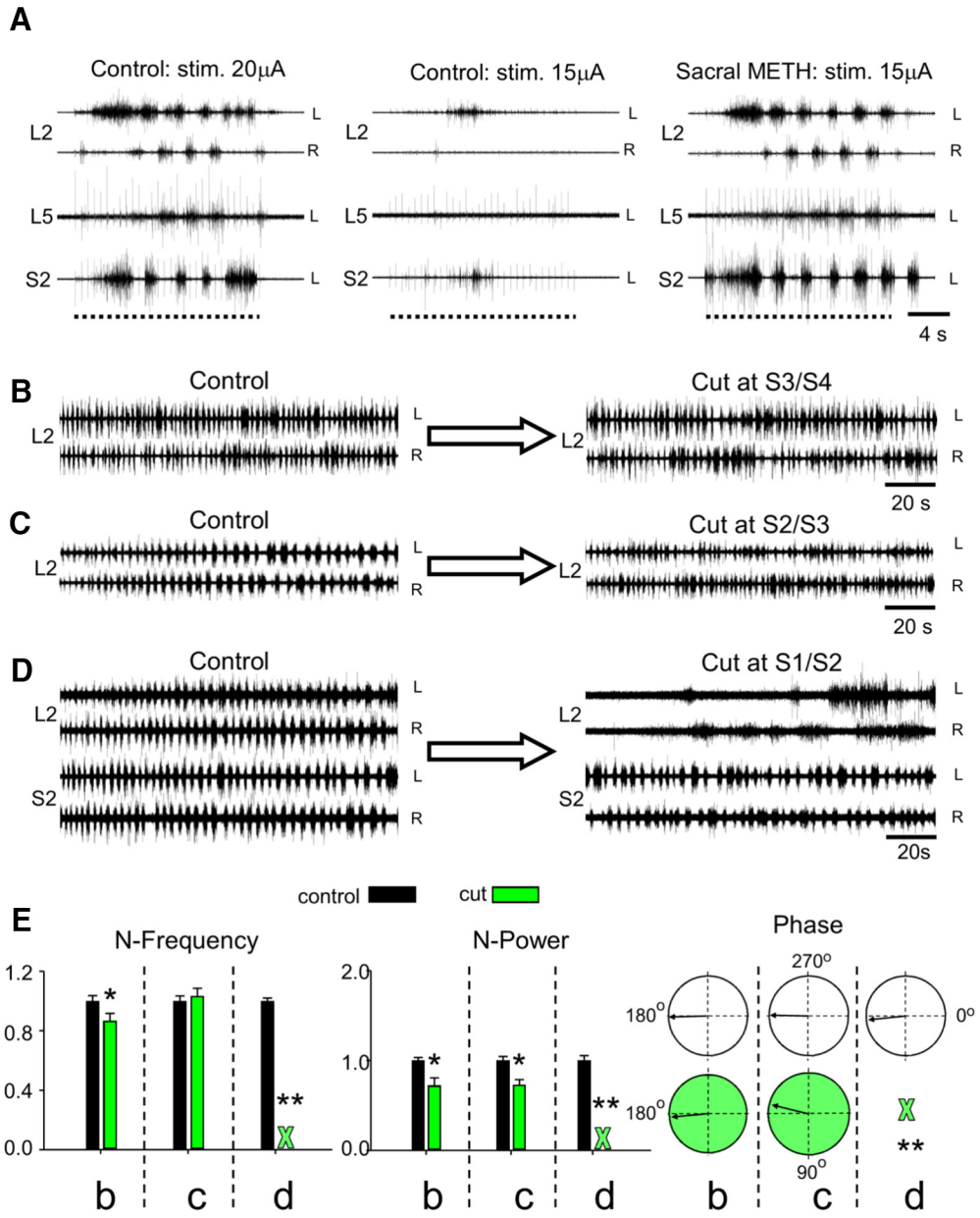

Figure 2. Effects of sacral METH on lumbar output during locomotor-like activity and studies of the segmental origin of the "fast" lumbar METH rhythm. ***A***, AC recordings (20 Hz to 10 kHz) from the left (L) and right (R) L2, and the left L5 and S2 ventral roots in response to 30-pulse, 1.66 Hz stimulus trains applied to the right L4 dorsal root at 20 (Control: stim. 20 μA) and 15 μA (Control: stim. 15 μA) before and after addition of 100 μM METH to the sacral compartment of a dual-chamber experimental bath (Sacral METH: stim. 15 μA). Dashed lines denote the duration of the stimulus trains. Note that sacral METH allowed the weak 15 μA stimulus to exceed the rhythmic threshold and to produce a robust locomotor-like rhythm. ***B***, ***C***, AC recordings (20 Hz to 10 kHz) of the METH rhythm from the left (L) and right (R) ventral roots of L2 before (***B***, ***C***, Control), and after cutting the cord at the S3/S4 or S2/S3 junctions (***B***, Cut at S3/S4; ***C***, Cut at S2/S3) in two different experiments. ***D***, AC recordings (20 Hz to 10 kHz) of the METH rhythm from the left (L) and right (R) ventral roots of L2 and S2 before (Control) and after cutting the cord through the S1/S2 junctions (Cut at S1/S2). Note the elimination of the fast L2 METH rhythm following separation of S2 from S1, while the fast METH rhythm persists in the detached sacral segments. The rhythm was produced by 100 μM METH. ***E***, Histograms of the mean ± SEM values of the normalized frequency (N-Frequency), normalized power (N-Power), and the mean left–right L2 phase and r-vector (Phase, circular plots) of the rhythm produced by 100 μM METH before (Control, black) and after (Cut, green) S3/S4 cut (5 experiments), S2/S3 cut (6 experiments), and S1/S2 cut (5 experiments). Green X denotes the abolition of the fast rhythm following the cut through S1/S2 junction. WT-based statistical analyses of the respective L2 time series in these experiments was used to calculate the mean quantitative indices (see Materials and Methods). For further details, see text. *, Significant difference between compared means. **, Block of the fast lumbar rhythm. All intersegmental cuts were between microscopically visible exits of caudal-most and rostral-most axons via ventral roots of the respective sacral segments.

and their location was defined with respect to the dye injection site and distance from the midline. Fluorophores were excited at the appropriate wavelength and images were acquired at 25–30 frames per second during neural activity induced by METH or SCA stimulation, and stored on the computer's hard disk using the Q Capture Pro software. The imaging and electrophysiological data were synchronized using transistor-to-transistor logic (TTL) pulses applied to initiate the electrophysiological data acquisition, open the shutter of the camera, start the image acquisition, trigger the stimulus trains in case of SCA stimulation, and finally close the shutter (for details, see Etlin et al., 2013).

Data acquisition and analyses. Electrophysiological data were digitized (Digidata 1320A, Molecular Devices) and stored on the computer's hard disk for subsequent analyses (Gabbay et al., 2002; Strauss and Lev-Tov, 2003; Gabbay and Lev-Tov, 2004; Etlin et al., 2010, 2013). All our electrophysiological and imaging data were analyzed using "Spinalcore," a menu-driven Matlab-based program, developed by Mor and Lev-Tov

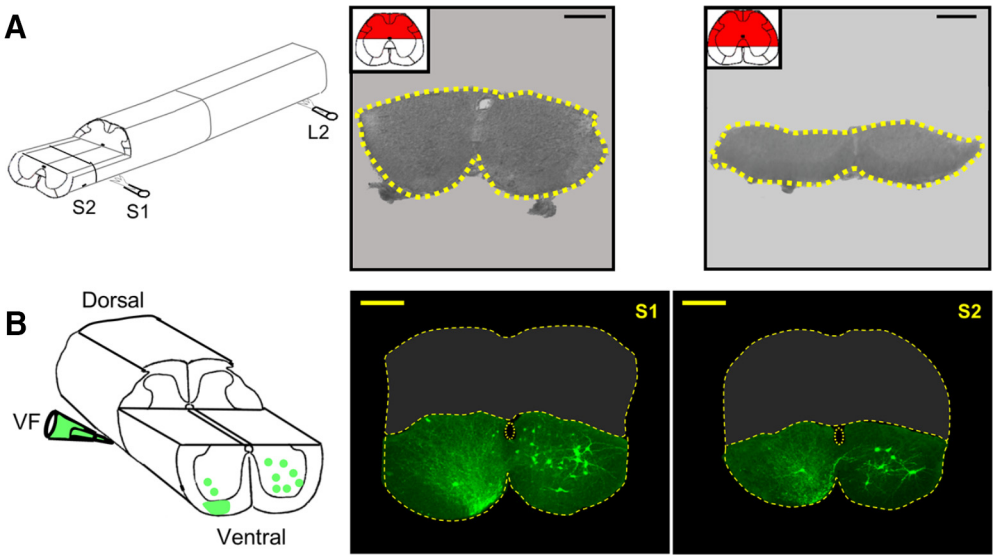

Figure 3. Dorsal lesions of S1/S2 and the neurons located below the lesions. ***A***, Schematic view of a spinal cord preparation following removal of S3-Co3 segments and the dorsal aspect of S1 and S2 segments (left). Confocal projected images of vibratome cross sections of fixed preparations cut through S2 after removal of the dorsal aspect of the cord to the level of the central canal (left micrograph, 100 μm thick) and below the level of the central canal (right micrograph, 200 μm thick). Sections were prepared following the physiological experiments (Fig. 4). Dashed yellow lines encircle the perimeter of the unlesioned part of the segments. Projected images of confocal *Z*-stacks were obtained using integrated laser scanning and conventional transmitted light Nomarski differential interference contrast. Calibration bars, 200 μm. ***B***, Schematic view of backfilling of cut VF axon bundles with fluorescein dextran at the left lumbosacral junction in an isolated spinal cord preparation following removal of the dorsal aspect of the S1–S2 segments to the level of the central canal (left). On the right are projected confocal images of sacral neurons labeled in S1 (left micrograph) and S2 (right micrograph) spinal segments through cut VF axons at the left lumbosacral junction in the dorsally lesioned preparation from which the dorsal parts of S1/S2 had been removed (as illustrated in the scheme). Calibration bars, 200 μm. The perimeter of the cross sections and the central canal are delineated by yellow dashed lines. The projected images are composed of 10 optical slices. Each slice is 8 μm thick. Eight hundred and twelve VFNs were labeled in S1 and S2 in the three experiments performed in this series; 93% of them had crossed lumbar projections, 57% of the VFNs were in lamina VIII and IX, while 43% of them were in lamina VII of the gray matter (for additional mapping experiments of sacral relay neurons with lumbar projections, see Etlin et al., 2010).

(2007), for electrophysiological and imaging signal processing and for stationary and nonstationary time-series analyses. To speed up the time-consuming calculations of the analyses, we exploited graphic processing unit-based parallel computing using the NVIDIA-developed Compute Unified Device Architecture (Mor et al., 2012a,b). Wavelet and wavelet-coherence analyses were performed to detect rhythmicity, determine the phase/power between the recorded time series in the time/frequency domain (Mor and Lev-Tov, 2007; Etlin et al., 2010, 2013), and to examine the relation between the optical and electrophysiological signals in the presence of METH or during SCA stimulation (Etlin et al., 2013). Full accounts of wavelet transform (WT)-based analyses have been previously reported (Mor and Lev-Tov, 2007; Etlin et al., 2010, 2013). Briefly, recorded data are high-pass filtered and rectified before WT-based analyses of the rhythm induced by METH or SCA stimulation. The quantitative indices of the rhythm, including the mean normalized crossed power (N-power), normalized frequency (N-frequency), coherence, and left–right phase shift (phase), are calculated from consecutive sampling epochs within the relevant high-power regions of interest of the coherent cross-power spectra of the examined time series (Mor and Lev-Tov, 2007; Etlin et al., 2010, 2013; Finkel et al., 2014). Since the fast METH rhythm stabilizes a few 10s of seconds after its initiation (Mor and Lev-Tov, 2007), our comparative analyses were performed after stabilization of the rhythm.

The statistical significance of the normalized indices of the rhythm (i.e., frequency, coherent power, and phase), extracted from WT analyses, was tested using conventional methods for comparisons of means in linear statistics (Student's *t* test, or factorial ANOVA and *post hoc* tests; Etlin et al., 2010, 2013). The statistical significance of the phase data was examined using circular statistics procedures for directionality (Rayleigh's test; Zar, 1999) and comparisons of the mean angles (the Watson–Williams *F* test; Zar, 1999).

The statistical analyses described above are demonstrated in Figure 1, which shows that fast lumbar METH rhythm produced in the rostral lumbar segments originates from the activated sacral neuronal networks. Addition of METH to the sacral compartment of the dual-chamber experimental bath produced the fast rhythm in the sacral and lumbar segments, while addition of METH to the lumbar compartment produces a very slow rhythm. Coherent cross-power density plots of the activity recorded following sacral and lumbar application of METH (*E* and *F*, respectively) show high-power (color-coded) frequency bands (heavy black lines) of the left L2 (LL2) versus right L2 (RL2) and RL2 versus RS2 time series shown in *C* and *D*. The mean ± SEM values of the frequency and power, and the mean phase shifts and r-vectors (insets) were extracted from 10 consecutive epochs of the respective high-power frequency bands of the spectra in *E* and *F*. Significant differences (two-way ANOVA, $F = 3{,}281{,}812$, $p \ll 0.0000001$ followed by Tukey's HSD $p \ll 0.0000001$) were found between the mean LL2-RL2 frequency following sacral (0.22 ± 0.0002 Hz) and lumbar (0.015 ± 0.00002) METH application.

The LL2-RL2 mean coherent cross-power values were 60 ± 5.9 (sacral METH) and 264.2 ± 11.5 (lumbar METH) and the RL2-RS2 cross-power values were 152.7 ± 7.2 (sacral METH) and 40.1 ± 2.2 (lumbar METH). Significant differences (two-way ANOVA, $F = 445.2$, $p \ll 0.0000001$, followed by Tukey's HSD $p < 0.00015$) were found between all the compared mean power values, except the means of LL2-RL2 and RL2-RS2 during sacral and lumbar METH ($p > 0.25$). The phase values were as follows: LL2-RL2: sacral METH, 180.6 ± 20.6°, r-vector = 0.94; lumbar METH, 170 ± 17.1°, r-vector = 0.96; RL2-RS2: sacral METH, 2.4 ± 9.9°, r-vector = 0.985; lumbar METH, 18.4 ± 23°, r-vector = 0.92.

Results

Sacral spinal networks activate lumbar METH rhythm

The α1-adrenoceptor agonist METH produces alternating left–right rhythmic bursts ("fast" METH rhythm) in sacral and lumbar flexor motoneurons when applied to the isolated spinal cord of the neonatal rat (Gabbay and Lev-Tov, 2004). Figure 1*A*,*B*, shows recordings from the left and right second lumbar and second sacral ventral root following bath application of 50 μM METH. The ~0.4 Hz alternating left–right rhythm persisted in

the lumbar and sacral segments for a long time. After surgically manipulating the spinal cord, Gabbay and Lev-Tov (2004) suggested that the rhythm originates in the sacral segments and the drive spreads rostrally to activate lumbar motoneurons. In Figure 1*C*,*D*, we mounted the isolated spinal cord in a dual-chamber experimental bath and examined the effects of specific application of METH to either the sacral or the lumbar compartments. Application of METH to the sacral compartment produced the "fast" METH rhythm (0.22 Hz in this case) in the sacral and rostral lumbar segments (Fig. 1*C*). Addition of METH to the thoracolumbar compartment after washing out the sacral METH generated a very slow (0.015 Hz) alternating left–right rhythm in the lumbar and sacral segments (Fig. 1*D*). Wavelet-based coherent cross-power spectra of the left and right L2 time series (LL2 vs RL2) and the right L2 and right S2 time series (RL2 vs RS2), in the presence of sacral or lumbar METH, are shown in Figure 1 *E*,*F*. The LL2 versus RL2 spectra (*E*, *F*, top) show the 14.7-fold decrease in frequency of the lumbar rhythm and the increase in the coherent crossed power (expressed as a darker red frequency band in *F* compared with *E*) in response to lumbar compared with sacral application of METH. In addition, the coherent crossed power of the RL2-RS2 time series was higher than that of LL2-RL2 during sacral application of METH (Fig. 1*E*, darker red frequency band in bottom vs top), whereas the crossed power of LL2-RL2 was higher than that of RL2-RS2 during lumbar application of METH (Fig. 1*F*, darker frequency band in top vs bottom). More details on statistical analyses of this experiment appear in Materials and Methods (Data acquisition and analyses).

We analyzed the lumbar time series (LL2-RL2) produced by sacral and lumbar application of METH in five experiments. The shared normalized frequency (N-frequency) of the rhythm produced by sacral application of METH decreased significantly from 1.00 ± 0.02 to 0.19 ± 0.02 (means ± SEM, $N = 5$, two-tailed *t* test; $t = 35$, $p \ll 0.000001$) after washing out the sacrally applied METH, and applying METH to the lumbar compartment. The mean normalized crossed power of the rhythm produced in the lumbar segments following sacral application of METH (N-power) was 1.00 ± 0.04. This increased significantly to 2.7 ± 0.53 (two-tailed *t* test; $t = -3.2$, $p < 0.0024$) after lumbar application of METH. This increased power reflects the appearance of slow massive lumbar bursts similar to those reported for noradrenaline-induced rhythms in the neonatal rat spinal cord (Gabbay and Lev-Tov, 2004). The mean left–right phase of the lumbar rhythm following sacral application of METH (180.5 ± 7°, r-vector = 0.99) did not differ from that obtained following lumbar application of METH (182.7 ± 16.8°, r-vector = 0.96; Watson–Williams *F* test, $F = 0.336$; $p > 0.57$). Another finding in this series was a decrease in the drive of the sacral rhythm during lumbar application of METH (Fig. 1*C*,*D*, compare S2 recordings). Analyses of the experiments performed in this series revealed that the N-power of the sacral rhythm decreased significantly from 1 ± 0.05 in the presence of sacral METH, to 0.37 ± 0.07 in the presence of lumbar METH (two-tailed *t* test; $t = 7.3$, $p \ll 0.000001$). This finding reflects the asymmetry of the direct sacral drive in the presence of sacral METH with the much weaker capacity of lumbar METH to drive the sacral segments in the absence of sacral METH.

In conclusion, the sacrocaudal segments of the spinal cord generate the "fast" rhythm in the presence of METH, and deliver the drive required to trigger the alternating left–right bursting in rostral lumbar segments.

To establish whether the increase in excitability of the rostral lumbar segments following sacral application of METH affects the lumbar motor output during the locomotor rhythm, we mounted the isolated spinal cords in a dual-chamber experimental bath, and elicited locomotor-like activity by stimulation of lumbar dorsal root afferents before and after addition of METH to the sacral compartment. Figure 2*A* shows that stimulation of the left L4 dorsal root at 20 μA produced locomotor-like rhythm recorded from the left and right L2, left L5, and left S2 ventral roots (Control: stim. 20μA). Because this and higher-intensity stimulation induced tonic firing after sacral application of METH (data not shown), we reduced the stimulation intensity to the threshold required to produce the rhythm or just below it, and recorded the responses before and after sacral application of METH. For example, stimulation of the L4 dorsal root at 15 μA failed to produce the rhythm (Control: stim. 15μA). However, repeating the 15 μA train after addition of METH to the sacral chamber produced a robust and regular rhythm (Sacral METH: stim. 15μA), comparable to the rhythm produce by the 20 μA pre-METH train (Control: stim. 20μA). The spontaneous METH rhythm was evident before the stimulus trains (data not shown) and in most cases was entrained during the trains and reinstated after their cessation. In some cases, a robust locomotor rhythm developed despite perturbations in the sacral rhythm during lumbar afferent stimulation. Analyses of the results obtained in five experiments revealed that N-power of the flexor LL2-RL2 series increased significantly from 1 ± 0.006 to 3.49 ± 0.48 ($t = -4.53$, $p < 000015$), and that of the flexor–extensor series (LL2-LL5/4) increased from 1 ± 0.1 to 2.97 ± 0.4 ($t = -2.77$, $p < 0.0076$) after addition of sacral METH. The N-frequency of the locomotor rhythm did not change significantly in the presence of sacral METH ($t = 1.96$, $p > 0.52$ for the LL2-RL2 time series; $t = -0.6$, $p > 0.55$ for the LL2-LL5/4 time series). The phase of LL2-RL2 changed from 178.6 ± 29°, r-vector = 0.88, to 170.0 ± 16°, r-vector = 0.96 ($F = 4.2$, $p < 0.043$, Watson–Williams *F* test) after sacral METH, while the LL2-LL5/4 phase changed from 173.2 ± 17.5°, r-vector = 0.96, before sacral METH to 167.6 ± 16°, r-vector = 0.97, after sacral METH, a difference that was not significant ($F = 1.7$, $p > 0.19$, Watson–Williams *F* test). Thus, sacral METH has the capacity to enhance the motor output produced during locomotor-like rhythm elicited by stimulation of lumbar afferents.

Ventral sacral networks lead to generation of the fast lumbar METH rhythm

To reveal the sacral networks responsible for generating the METH rhythm and relaying the drive to the rostral lumbar segments, we performed electrophysiological recordings from sacral and lumbar ventral roots, and took confocal and calcium images of spinal neurons. These were combined with surgical and pharmacological manipulations of the isolated spinal cord of the neonatal rat.

In the first series of 15 experiments (Fig. 2*B*–*E*), we examined the effects of removing different sacrocaudal segments on the ability of METH to produce the "fast" lumbar METH rhythm. Recordings of the lumbar METH rhythm are shown before and after transecting the cord at the S3/S4, S2/S3, and S1/S2 junctions (Fig. 2*B*–*D*). The "fast" METH rhythm persisted in the rostral lumbar segments after transecting the spinal cord at the S3/S4 (Fig. 2*B*) or S2/S3 junction (Fig. 2*C*), but was blocked after cutting the cord through the S1/S2 junction (Fig. 2*D*, L2 recordings in cut at S1/S2). The fast S2 rhythm, simultaneously recorded from LS2 and RS2 ventral roots, persisted with no major changes after the S1/S2 cut (Fig. 2*D*, S2 recordings in cut at S1/S2).

Figure 2*E* summarizes the effects of these surgical manipulations on the N-frequency, N-power, and the left–right phase of

the METH lumbar rhythm recorded from L2 ventral roots before and after the S3/S4, S2/S3, and S1/S2 cuts (Fig. 2*E*). The S3/S4 and S2/S3 cuts did not impair the fast lumbar METH rhythm, although some effects were noticed. N-frequency decreased slightly after cut at S3/S4 (~13%, $t = 2.2$, $p < 0.03$) and did not change after cutting at S2/S3 ($t = 0.5$, $p > 0.6$). N-power decreased (~28%; $t = 3.1$, $p < 0.003$ after cut at S3/S4; $t = 3.7$, $p < 0.0005$ after cut at S2/S3), probably due to removal of the contribution of S3 and S4 neurons to the ascending drive. The LL2-RL2 phase did not change significantly after S3/S4 and S2/S3 cuts ($F = 2.8$, $p > 0.1$, Watson–Williams F test). However, cutting through the S1/S2 junction caused a dramatic effect. The fast lumbar rhythm was blocked (green X in the histograms) and replaced by slow nonrhythmic bursting in three of five experiments and by a slow alternating left–right rhythm in two of five experiments. In these two experiments, the N-frequency decreased ninefold ($t = 19.5$, $p \ll 0.0000001$), and N-power increased 86% ($t = -2.7$, $p < 0.02$) due to the appearance of slow massive bursts in L2. The phase was not changed (before S1/S2 cut: 174.8°± 13.0°, r-vector = 0.97; after S1/S2 cut: 164.7°±30.1°, r-vector = 0.87; $F = 0.88$, $p > 0.3$, Watson–Williams F test).

Analyses of the fast S2 rhythm, simultaneously recorded from LS2 and RS2 ventral roots before and after the S1/S2 cut, revealed that the N-frequency of the rhythm changed from 1 ± 0.01 to 1.12 ± 0.05 after the lesion ($t = -1.9$, $p > 0.06$). Similar changes in N-frequency of the S2 METH rhythm were observed after cutting through the L6/S1 joint (Gabbay and Lev-Tov, 2004). Thus, the variable changes in frequency most likely result from removal of descending influence of the lumbar cord. The mean N-power changed significantly from 1 ± 0.03 to 0.56 ± 0.09 ($t = 4.8$, $p < 0.00002$) after the cut and the LS2-RS2 phase shift was not changed after the S1/S2 cut (before cut: 178 ± 8.3, r-vector = 0.99; after cut: 180.9 ± 5.0, r-vector = 0.99; $F = 1.9$, $p > 0.17$, Watson–Williams F test). The reduction in power reflects the damage caused by cutting through the rostral border of the recorded S2 segment.

The experiments described above indicated that continuity between the lumbar cord and at least the first two sacral spinal segments is required for generating the fast lumbar METH rhythm.

Next, we determined the range and extent of the S1-S2 gray matter critical for producing the fast lumbar METH rhythm. In another series of 18 experiments, we transected the cord at the S2/S3 junction. Then, we progressively removed parts of the dorsal aspect of the S1-S2 segments in different experiments (Fig. 3*A*), and examined the ability of METH to produce the "fast" rhythm in the rostral lumbar segments before (Fig. 4*A1–A4*) and after (Fig. 4*B1–B4*) the dorsal lesions.

Figure 4*A*,*B* shows the METH rhythm in rostral lumbar segments in four different experiments (1–4). The fast rhythm persisted after moderate dorsal lesions of S1-S2 (Fig. 4, compare *A1*, *A2*, *B1*, *B2*), and even after a more severe dorsal lesion (removal of the dorsal aspect of S1-S2 down to the level of the central canal; Fig. 4*B3*). However, extending the S1-S2 dorsal lesion below the central canal (Figs. 3*A*, right, 4) blocked the "fast" lumbar METH rhythm and produced, in this case, slow nonrhythmic bursting (Fig. 4, compare *A4*, *B4*). The means ± SE of the N-frequency (N-freq), coherent crossed power (N-power), and left–right phase (phase), extracted from WT and WT-coherence-based analyses (see Materials and Methods) of the lumbar METH rhythm in the individual experiments demonstrated in Figure 4*A*,*B* are shown in Figure 4*C* (control, black histograms; lesioned, green histograms). The N-frequency of the experiments with the lesions shown in *B1*, *B2*, and *B3* changed significantly compared with control (one-way ANOVA, $F = 321$, $p \ll 0.0001$, followed by Tukey's N-HSD, $p < 0.00001$), until the fast rhythm was blocked following the lesion shown in *B4*. The mean N-power did not change significantly following the lesion in *B1*, and then decreased significantly following the lesions in *B2* and *B3*. In *B4* the mean N-power was completely blocked (one-way ANOVA, $F = 64.5$, $p \ll 0.00001$, N-HSD Tukey's $p < 0.00001$). The means of the left–right phase of the fast L2 rhythm did not change significantly from their respective control values after the *B1*, *B2*, and *B3* lesions (Watson–Williams F test: *B1*, $F = 4.26$, $p > 0.07$; *B2*, $F = 3$, $p > 0.12$; *B3*, $F = 2.9$, $p > 0.13$). After the *B4* lesion, the rhythm was blocked.

Statistical analyses of 12 dorsal lesion experiments in which the dorsal aspect of S1-S2 was removed down to the level of the central canal revealed that the fast lumbar METH rhythm persisted in each one of them following the lesion. The mean N-frequency of the lumbar rhythm following the lesion in these experiments (0.95 ± 0.05) did not differ from that of the prelesion control (1 ± 0.017; $t = 0.96$, $p > 0.33$). The N-power decreased after the lesion from 1 ± 0.027 to 0.75 ± 0.054 ($t = 4.16$, $p < 0.00006$), and the left–right phase was unaltered (control: 178.3 ± 8.7°; r-vector = 0.99; lesioned: 174.2 ± 13.3°, r-vector = 0.97). In contrast, in the series of experiments in which the dorsal aspect of S1 and S2 was removed to below the central canal ($N = 4$), the fast METH rhythm ceased; it was replaced by slow nonrhythmic bursting in two experiments, and by a slow and bilaterally synchronous rhythm in two other experiments. In these latter experiments, the N-frequency decreased by a factor of 17.9 from 1 ± 0.04 to 0.056 ± 0.009 ($t = 16.8$, $p \ll 0.0000001$). The N-power (1 ± 0.093) did not change after the lesion (1.05 ± 0.26; $t = -0.196$, $p > 0.84$) and the LL2-RL2 phase changed significantly from 176.8 ± 2.1°, r-vector = 0.99, to 348.3 ± 3.1°, r-vector = 0.98 (Watson–Williams F test, $F = 2110$, $p \ll 0.0000001$).

Interestingly, unlike the slow alternating rhythm produced by lumbar application of METH (Fig. 1), the elimination of the fast lumbar rhythm resulting from the surgical manipulations (Figs. 2, 4*B4*) led to the appearance of variable slow nonlocomotor or nonrhythmic bursting. We suggest that the ascending sacral drive contributes to the regularity of the slow lumbar METH rhythm, and that impairment of this drive can perturb the left–right phasing of the slow METH (or noradrenergic) lumbar rhythm. This argument is supported by the appearance of perturbed phasing of the slow alternating rhythm induced by lumbar application of METH after blocking synaptic transmission in the sacral segments by applying low-calcium ACSF containing CNQX and APV (M. Cherniak, A. Lev-Tov, and L. Anglister, unpublished observations).

To further define the extent of S1 gray matter required for generating the METH rhythm in the rostral lumbar segments, we transected the cord at the S2/S3 junction in three experiments, and then removed the dorsal aspect of S1 to just below the central canal (Figs. 3*A*, right, 5*B*, top), while leaving the S2 segment intact. The METH rhythm observed in the prelesioned preparation (Fig. 5*A*) was not blocked after the lesion (Fig. 5*B*). Statistical analyses of these experiments ($N = 3$) revealed that the N-frequency of the lumbar METH rhythm (1.0 ± 0.018) was not affected by the lesion, displaying a value of 1.1 ± 0.05 ($t = -1.6$, $p > 0.11$). The same was true for the left–right L2 phase (prelesion control: 180.8 ± 11°, r-vector = 0.98; post-S1 lesion: 176.9 ± 15.7°, r-vector = 0.96; Watson–Williams F test, $F = 1.0$, $p > 0.32$). However, the N-power of the prelesion control (1 ± 0.03) was reduced to 0.51 ± 0.05 ($t = 8.73$, $p \ll 0.0000001$) after

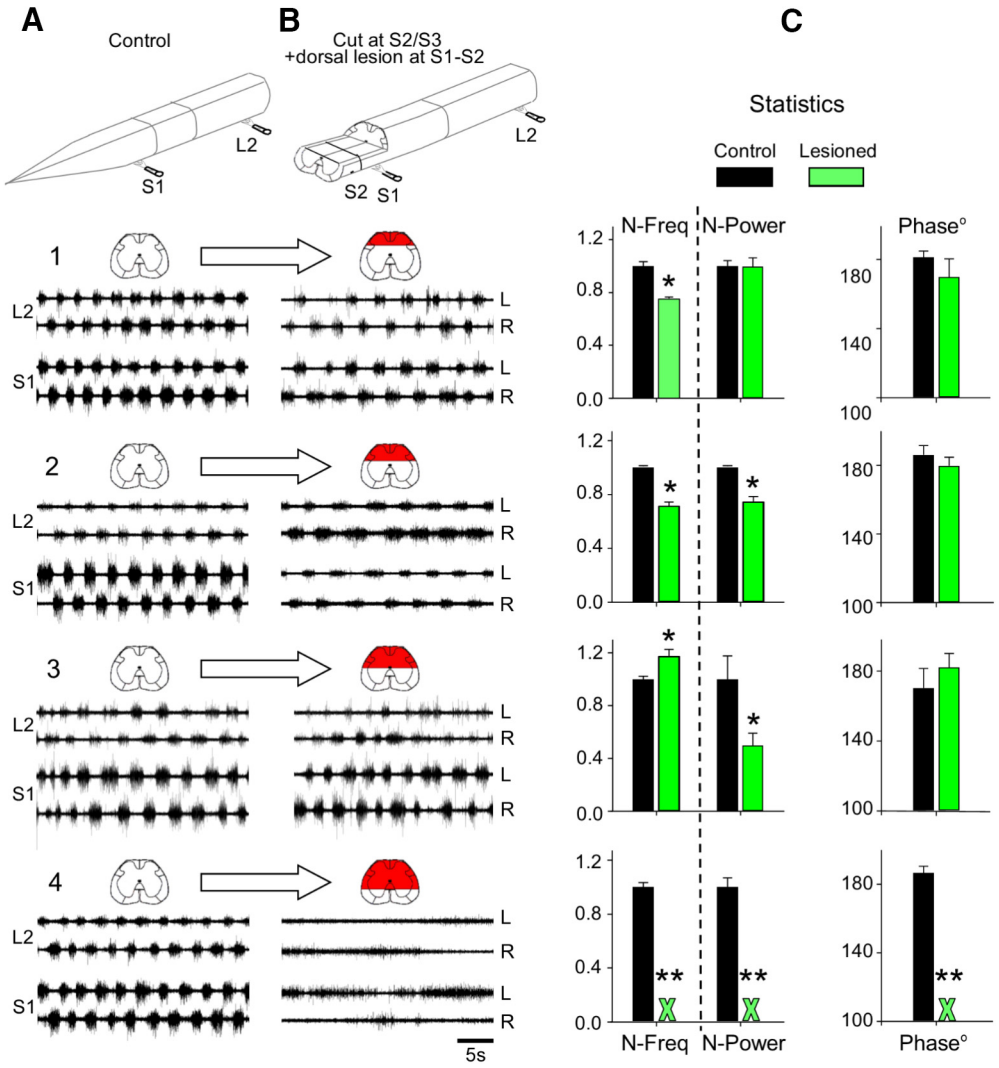

Figure 4. The "fast" lumbar METH rhythm persists after S2/S3 cut and removal of the dorsal aspect of S1 and S2 down to, but not below, the central canal. ***A***, ***B***, AC recordings (20 Hz to 10 kHz) from the left (L) and right (R) ventral roots of S1 and L2 before (***A***, Control, 1–4) and after transecting the cord at the S2/S3 junction, and removing increasing parts of the dorsal aspect of S1 and S2 in four different experiments (***B***, Cut at S2/S3; dorsal lesion at S1–S2, 1–4). Bath application of 100 μM METH generated the recorded rhythm. The prelesion and postlesion preparations are illustrated above the respective recordings. The red marked regions in the schematic cross sections denote the extent of the lesions. The fast lumbar METH rhythm stops only when dorsal lesion extends below the central canal (4). ***C***, Histograms of the mean ± SEM values of the normalized frequency (N-Frequency), normalized power (N-Power), and the mean left–right L2 phase of the individual experiments (***A***, ***B***, 1–4) before (Control, black) and after each lesion (Lesioned, green). Green X = block of the fast lumbar rhythm (normalized frequency, power, and phase indices). Statistical details in text. *, Significant difference between compared means. **, Block of the fast lumbar rhythm.

removal of most of the S1 gray matter, indicating that the lesion eliminated some of the sacral neurons that contribute to the drive produced by the sacral circuitry.

Moreover, in three additional experiments, we showed that the METH rhythm was perturbed but not abolished when the dorsal aspect of S1 was removed to below the central canal and even after additional removal of the dorsal aspect of the S2 segment to the level of the central canal (Fig. 5*C*,*D*). The normalized frequency did not change after lesion (control: 1.0 ± 0.024; lesioned: 0.95 ± 0.07; $t = 0.62$, $p > 0.53$). The mean left–right L2 phase also persisted after lesion (control: 179 ± 12.2°, r-vector = 0.978; lesioned: 193.1 ± 40.9°, r-vector = 0.775; Watson–Williams F test, $F = 1.61$, $p > 0.21$), while the N-power decreased from 1.0 ± 0.072 to 0.56 ± 0.046 ($t = 5.14$, $p < 0.00002$).

In summary, the series of experiments described in Figures 1–5 showed that the METH rhythm originates in the sacral segments and that the networks residing in S2 ventral to the central canal are sufficient to generate this rhythm and to deliver the drive, producing the 0.15–1 Hz bursting in the rostral lumbar segments.

Sacral neurons with direct lumbar VF projections mediate the lumbar METH rhythm

After revealing the sacral gray matter regions critical for producing the rhythmic bursts in rostral lumbar motoneurons in the presence of METH, we aimed to determine the connectivity that links the sacral and rostral lumbar segments during the METH rhythm.

To this end, specific white matter funiculi were lesioned at the lumbosacral junction and the ability to produce the rostral rhythm was compared with that of the prelesion control (six experiments). Figure 6*A* shows that it is possible to induce the "fast" METH rhythm in the rostral lumbar segments when the VF are bilaterally intact and the rest of the white matter funiculi are cut bilaterally (Fig. 6*A*, control to L6/S1: only bilateral VF intact). The mean indices of the rhythm in the prelesion control were as

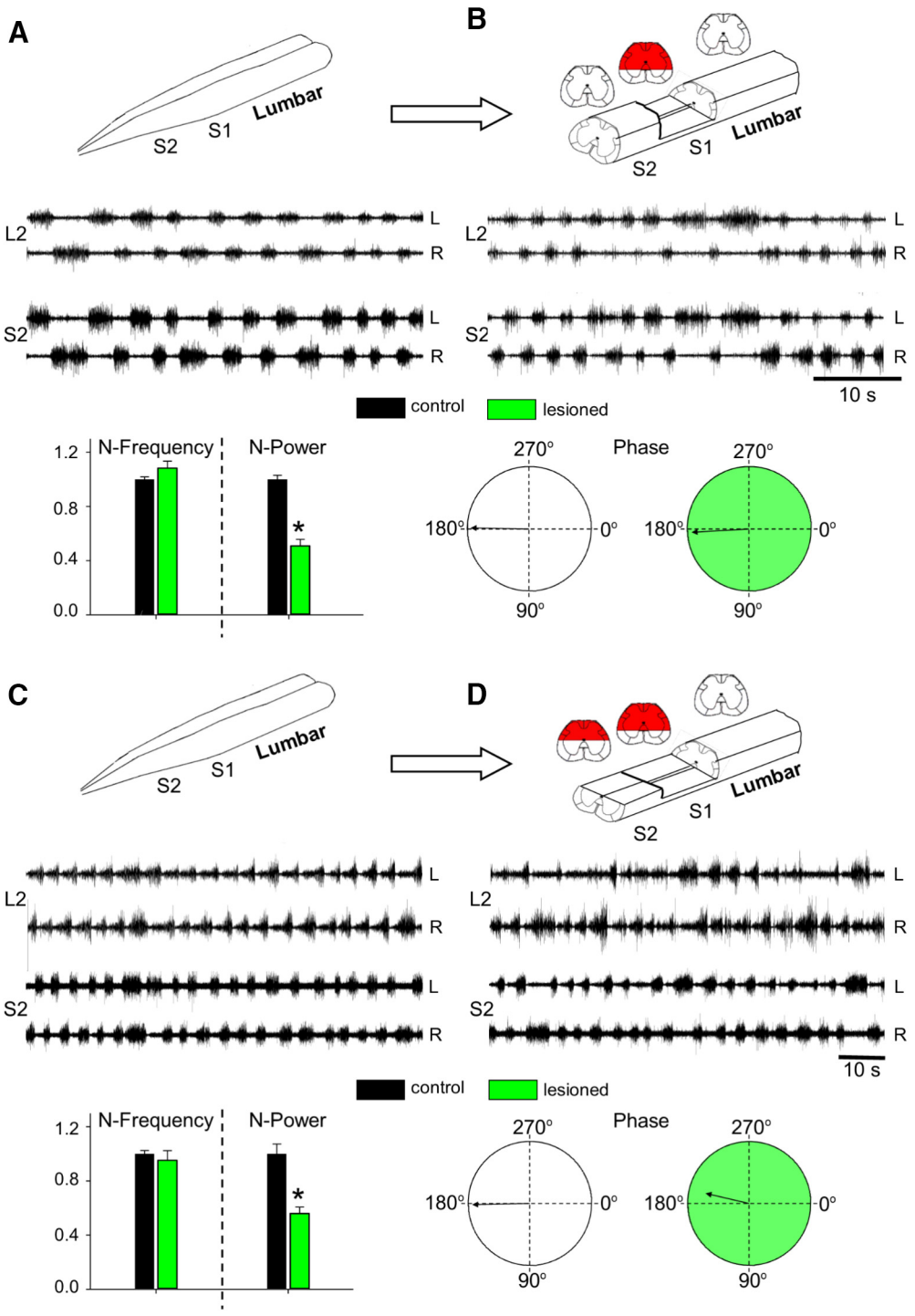

Figure 5. The ventral aspect of S2 is sufficient to produce the "fast" lumbar METH rhythm when the dorsal aspect of S1 is removed. AC recordings (20 Hz to 10 kHz) from the left (L) and right (R) ventral roots of S2 and L2 in the presence of METH (100 μM). ***A***, ***B***, Recordings before (***A***) and after (***B***) transecting the cord at the S2/S3 junction, and removing the dorsal aspect of S1 below the central canal. ***C***, ***D***, The fast lumbar rhythm produced by bath-applied METH (***C***) persisted after transecting the cord at the S2/S3 junction, removing the dorsal aspect of S1 below the central canal, and removing the dorsal aspect of S2 down to the central canal (***D***). Superimposed below the recordings in ***A–D*** are histograms of the mean ± SEM values of the N-frequency, N-Power, and the mean LL2-RL2 phase and r-vector before (Control, black) and after the lesions (Lesioned, green) in the five (***A***, ***B***) and three (***C***, ***D***) experiments performed in this series. *, Significant differences between the compared means. Schematic illustrations of the prelesion and postlesion preparations appear above the respective recordings in ***A–D***. The red regions in the schematic cross sections denote the extent of the lesions.

follows: N-frequency, 1.00 ± 0.026; N-power, 1.00 ± 0.035; left–right L2 phase, 180.8 ± 7.3°, r-vector = 0.99. The mean indices following the lesion were as follows: N-frequency, 0.92 ± 0.035; N-power, 1.05 ± 0.086; and left–right L2 phase, 180.9 ± 8.1°, r-vector = 0.99. There were no significant differences between the control and the corresponding post-lesion indices (N frequency: $t = 1.86$, $p > 0.07$; N-power: $t = -0.51$, $p > 0.61$; phase: $F = 0.0008$, $p > 0.97$). In contrast, bilateral interruption of the VF in a different series of six experiments abolished the "fast" METH rhythm in the rostral lumbar segments (Fig. 6*B*, L6/S1: VF bilat-

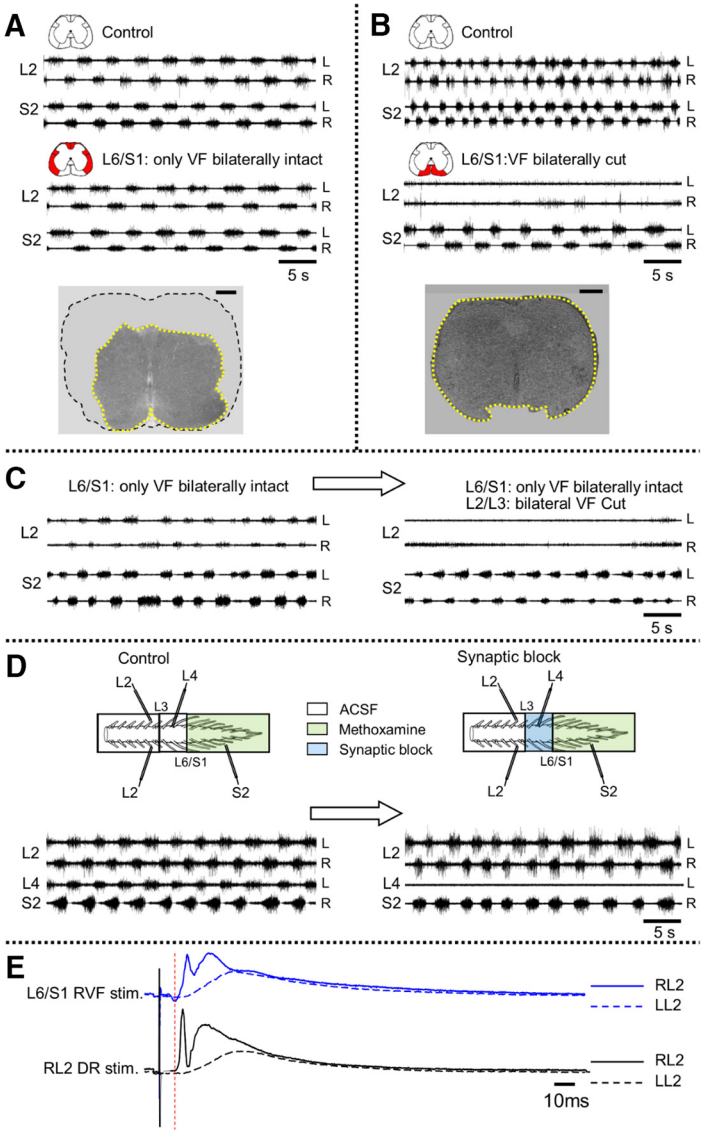

Figure 6. Sacral relay neurons with direct lumbar projections through the ventral white matter funiculi mediate the "fast" lumbar METH rhythm. ***A***, AC recordings (20 Hz to 10 kHz) of the METH (100 μM) rhythm, from the left (L) and right (R) ventral roots of S2 and L2, before (Control) and after interruption of all the white matter funiculi excluding the VF (L6/S1: only VF bilaterally intact). ***B***, Recording (as in ***A***) before (Control) and after a bilateral interruption of the VF at L6/S1 junction while leaving the rest of the white matter funiculi uninterrupted (L6/S1: VF bilaterally cut). The bilateral VF lesion blocked the lumbar rhythm induced by the METH (***A***), while the bilateral interruption of the VLF, LF, DLF, and DF (***B***) had no significant effect on the lumbar rhythm (see text). Red marked funiculi in the schematic insets in ***A*** and ***B*** denote the extent of the lesions. Histological examination of cross sections cut through the lumbosacral junctions show the microscopic location and extent of the lesions (***A***, bottom: bilateral interruption of the VLF, LF, DLF, and DF; ***B***, bottom: bilateral interruption of the VF). Serial 20-μm-thick cross sections of paraffin-embedded preparations visualized using light microscopy (Etlin et al., 2010) were used to compose the micrographs. ***C***, The rhythm induced by 100 μM METH (recorded as in ***A***) in a preparation with the VF as the only bilaterally intact funiculus before (L6/S1: only VF bilaterally intact) and after bilateral interruption of the VF at the L2/L3 junction (L6/S1: only VF bilaterally intact; L2/L3: bilateral VF cut). ***D***, The "fast" METH lumbar rhythm is produced by activation of sacral relay neurons with direct ascending projections to the rostral lumbar segments. A schematic illustration of the experimental setting is shown at the top. The preparation is mounted ventral side up in a tripartite experimental bath with a rostral (T6 to caudal L2), middle (caudal L2 to rostral S1), and sacrocaudal (S1 to Co3) compartments separated by Vaseline walls. AC recordings (20 Hz to 10 kHz) are obtained from the left (L) and right (R) L2, the left L4, and the right S2 ventral roots. Recordings (as in ***A–C***) are shown before (Control) and after blocking synaptic transmission in the middle compartment by changing its bathing medium to low-Ca^{+2}/high-Mg^{+2} ACSF containing 10 μM CNQX and 20 μM APV (Synaptic block, blue). The lumbar synaptic block (no L4 activity) does not interfere with the fast lumbar rhythm (L2 activity) induced by METH-activated (green) sacral networks and sacral relay neurons. ***E***, Stimulation of sacral projections through the VF elicits short-latency synaptic responses in L2 motoneurons. AC recordings (20 Hz to 10 kHz) of VRPs from the right (solid line) and left (dashed line) L2 ventral root in response to stimulation of cut VF axon bundles at the right lumbosacral junction (blue) and the right L2 dorsal root (black). The bathing medium contained 1 mM mephenesin. All responses were elicited by 0.05 Hz repetitive stimulation at 125 and 25 μA for the right VF-induced and dorsal root (DR)-induced VRPs, respectively. Red thin dashed line denotes the monosynaptic latency of the DR-induced RL2 VRP. For further details, see text.

erally cut), converted it to slow nonrhythmic bursting in four experiments, and to a slow alternating left–right rhythm in two other experiments. In these two latter experiments, the N-frequency decreased postlesion by ~7-fold (from 1 ± 0.05 to 0.14 ± 0.06, $t = 23.5$, $p \ll 0.0000001$), but the N-power did not change (prelesion, 1 ± 0.093; postlesion, 1.05 ± 0.26; $t = -0.19$, $p > 0.84$). Likewise, the LL2-RL2 phase in these two experiments remained unaltered (prelesion: 178.8 ± 17°, r-vector = 0.97; postlesion: 175.3 ± 12.9°, r-vector = 0.97; Watson–Williams F test, $F = 0.2$, $p > 0.65$).

Thus, the two series of experiments displayed in Figure 6*A*,*B* show that the drive required to produce the fast lumbar METH rhythm spreads from the sacral to the lumbar segments only through the VF of the white matter. It should be noted that this differs from the SCA activation pathways that travel also through the ventrolateral funiculi (VLFs), the lateral funiculi (LFs), and the dorsolateral funiculi (DLFs).

The next question we asked concerned the connectivity between the ascending VF projections from the sacral segments and their targets in the rostral lumbar segments of the spinal cord. In an earlier study, we showed that sacral relay neurons activated by stimulation of SCAs could initiate the locomotor rhythm via direct VF projections and also by serial recruitment of propriospinal neurons interposed between short projecting VFNs and the LCPGs (Etlin et al., 2010). To clarify whether the same rules apply to the METH-activated sacral VFNs, we performed two series of experiments. In the first series ($N = 4$), we interrupted the white matter funiculi at the L6/S1 junction while leaving the VF bilaterally intact. We then disconnected the VF at the rostral lumbar level (L2/L3) and examined the capacity of METH to produce the fast lumbar rhythm. Figure 6*C* shows that the fast lumbar METH rhythm produced in preparations with VF as the only bilaterally intact funiculi at the lumbosacral junction (Fig. 6*C*, L6/S1: only VF bilaterally intact) was transformed into a slow nonrhythmic pattern in two of four experiments, and into a very slow rhythm in the two other experiments, after interrupting the VF at the L2/L3 junction (Fig. 6*C*, L6/S1: only VF bilaterally intact, L2/L3 bilateral cut VF). The N-frequency in these two latter experiments decreased after lesion from 1 ± 0.02 to 0.2 ± 0.02 ($t = 16.5$, $p \ll 0.0000001$), but the N-power of the rhythm (1 ± 0.07) did not

change (1.8 ± 0.5; $t = -1.66$, $p > 0.1$). The LL2-RL2 phase of one of these experiments (phase: $174.9 \pm 8.4°$, r-vector = 0.99) did not change after the lesion ($162.3 \pm 17.7°$, r-vector = 0.95; Watson–Williams F test, $F = 1.77$, $p > 0.22$). However, the METH rhythm of the other experiment became bilaterally synchronous after the lesion under these conditions, as reflected in the LL2-RL2 phase change (prelesion: $179.5 \pm 7.2°$, r-vector = 0.99; postlesion: $9.3 \pm 10.2°$, r-vector = 0.98; Watson–Williams F test, $F = 619$ $p \ll 0.0000001$).

This series of experiments suggested that generation of the fast lumbar METH rhythm requires activation of sacral VFNs with direct projections to the rostral lumbar segments, and does not involve serial chain recruitment of propriospinal neurons.

To further test this suggestion, we designed a second series of experiments ($N = 5$), in which we applied METH to the sacral segments, blocked synaptic transmission along most of the lumbar segments, and examined whether the fast METH rhythm was generated in the rostral lumbar segments under these conditions (Fig. 6*D*). The preparation was mounted in a triple-chamber experimental bath (Fig. 6*D*, top) made up of a rostral (L2 and up), middle (cauda-L2 to caudal-L6), and sacrocaudal compartment (S1 and down). We found that the METH rhythm induced in the rostral lumbar compartment by application of METH to the sacral compartment (Fig. 6*D*, control) was not impaired if synaptic transmission along the caudal-L6 to caudal-L2 segments was blocked. This synaptic block was obtained by switching the bathing medium in the middle chamber from ACSF to low Ca^{+2}/high Mg^{+2} ACSF containing CNQX (10 mM) and APV (20 mM) (Fig. 6*D*, Synaptic block). The effectiveness of the synaptic block in the middle compartment was demonstrated by the abolition of L4 ventral root activity in response to SCA stimulation (data not shown). Occasionally, depending on the proportion of flexor motoneurons in L4 (Gabbay and Lev-Tov, 2004), METH could induce the fast rhythm also in L4 (see Fig. 6*D*, Control). In this latter case, the L4 METH rhythm was abolished by application of the blocking mixture to the middle compartment (Fig. 6*D*, Synaptic block). Statistical analyses of the results obtained in the five experiments performed in this series revealed that during the synaptic block, the N-frequency of the lumbar METH rhythm increased (from 1.00 ± 0.026 to 1.15 ± 0.05; $t = -3.0$, $p < 0.004$), the N-power decreased (from 1 ± 0.05 to 0.78 ± 0.04; $t = 3.38$, $p < 0.0014$), and the mean LL2-RL2 phase remained unaltered (control: $175.6 \pm 12.1°$, r-vector = 0.98; synaptic block: $181.9 \pm 12.5°$, r-vector = 0.98; Watson–Williams F test, $F = 3.1$, $p > 0.08$).

The two series of experiments displayed in Figure 6*C*,*D* showed that the METH rhythm produced in the rostral lumbar segments depended on the continuity along the sacral and lumbar VF, and that most likely it did not involve serial recruitment of lumbar propriospinal neurons interposed between the sacral networks and the rostral lumbar circuitry. The results of these experiments strongly suggest a direct mono/oligosynaptic coupling between the sacral relay neurons and the rostral lumbar segments. To examine whether such coupling exists, we compared in four experiments the ventral root potentials (VRPs) produced in rostral lumbar motoneurons by stimulation of cut VF axons at the lumbosacral junction to those produced in the same motoneurons by stimulation of the homonymous dorsal root. Figure 6*E* shows that the VF-induced L2-VRPs (solid blue line) had comparable latencies to the monosynaptic reflex evoked in L2 by stimulation of the L2 dorsal root (solid black line), despite the much longer conduction path (four spinal segments) of the VF axons to the target motoneurons. Moreover, the latency of the ipsilateral VF VRPs was much shorter than that of the contralateral L2 VRPs elicited under the same conditions by stimulation of the ipsilateral VF (dashed blue line) or dorsal root (dashed black line). The mean latency of the ipsilaterally evoked VF VRPs in four experiments was 9.3 ± 2.1 ms in the presence of the polysynaptic blocker mephenesin (Floeter and Lev-Tov, 1993; Pinco and Lev-Tov, 1994; Kasumacic et al., 2010), while that of the monosynaptic L2-reflex was 7.4 ± 1.1 ms. Thus, after subtraction of the mean conduction time (1.6 ± 0.3 ms) measured by stimulating cut VF axons at the lumbosacral junction and recording from cut VF axons at the L1/L2 junction, at the end of one of the experiments, the corrected latency of the VF VRPs (7.53 ms) was comparable to that of the monosynaptic reflex. The latency of the contralateral VRPs recorded at the same time was 11.4 ± 1.6 and 16.3 ± 4.7 ms for the dorsal and VF-evoked VRPs, respectively. Although the current spread from the stimulating VF electrode may have shortened a bit the VF VRPs, and despite the fact that mephenesin did not completely block polysynaptic transmission, the small differences between the latency of VF-induced L2 VRPs and that of the monosynaptic L2 reflex support the suggested mono/oligosynaptic connectivity between ascending VF projections from the sacral segments and rostral lumbar motoneurons.

METH induces rhythmic discharge in sacral VFNs

The experimental results described so far in the present study suggest that rostrally projecting sacral VFNs residing in the ventral aspect of S1/S2 gray matter play a major role in delivering the drive required for producing the fast lumbar METH rhythm. Therefore, the next part of our study aimed to identify sacral neurons with ascending projections through the VF that respond to METH, and examine whether their activity correlates with the concurrent motor output produced in the presence of METH. To this end, we back-labeled sacral VFNs with crossed and uncrossed lumbar projections (Fig. 7*A*,*B*) with the indicator Calcium Green dextran through cut VF axon bundles at the lumbosacral junction, imaged changes in fluorescence produced by calcium transients in labeled sacral neurons, and recorded the concurrent motor output in the presence of METH in the en bloc preparation. A scheme of the preparation, the recordings and imaging arrangements is shown in Fig. 7*A1* (see legend for more details).

Figure 7*A2* shows the rhythmic discharge recorded from the S2 and L2 ventral roots in the presence of METH and the three 20 s TTL pulses used to open the CCD shutter for calcium imaging of a sacral VF neuron with crossed lumbar projections in one of the experiments. The left S1 VF neuron (Fig. 7*A3*) was labeled from cut VF axons at the right lumbosacral junction. The activity produced by METH in this VF neuron (Fig. 7*A4*, $\Delta F/F$; see Materials and Methods) was imaged during the second opening of the CCD shutter (Fig. 7*A2*, green-shaded area), simultaneously with the concurrent electrophysiological recordings of the motor output. The mean reference image (F, ~10-frame average) was sampled just before the appearance of a regular METH rhythm (immediately after opening of the shutter in the presence of METH; Fig. 7*A2*, blue dashed line).

Wavelet-based calculation of the phase shift between the optical and electrophysiological signals (see Materials and Methods) revealed that the activity of this imaged VFN was in phase ($340.98 \pm 1.15°$, r-vector = 1) with the concurrent rhythmic motor output ipsilateral (left L2) to the soma of the imaged neuron. Figure 7*B* shows L2 and S2 ventral root recordings and simultaneous imaging of a sacral VF neuron with uncrossed lumbar projections during the METH rhythm. Backfilled from the

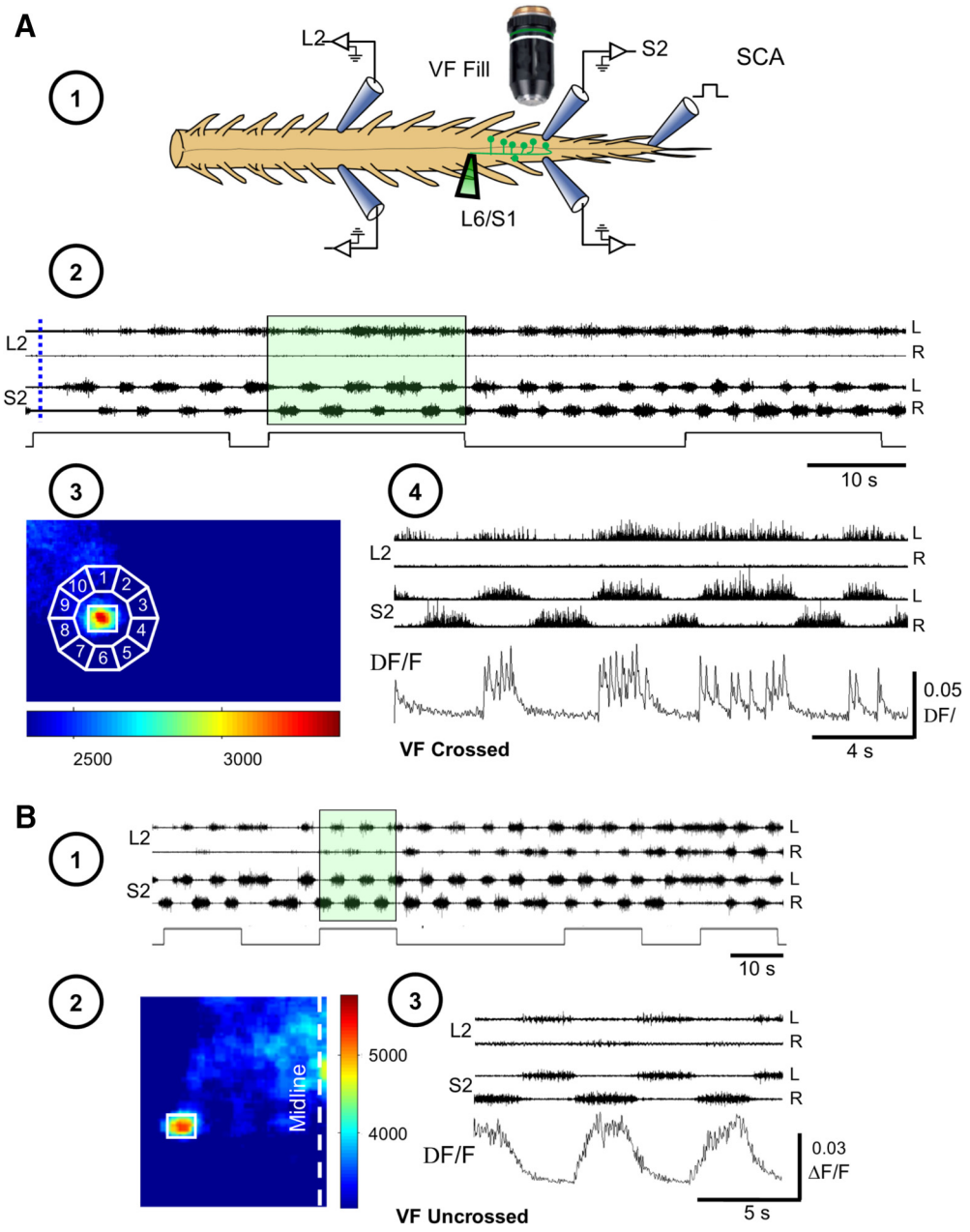

Figure 7. Calcium imaging of the discharge of sacral VFNs during the "fast" METH rhythm. ***A***, Imaging from a sacral VFN with crossed lumbar projections. ***A1***, Illustration of the experimental setup used for simultaneous imaging of a VFN and electrophysiological recordings of the motor output during the rhythm produced by bath application of METH. Sacral relay neurons are loaded with Calcium Green dextran through the cut VF at the lumbosacral junction (L6/S1) in the isolated spinal cord preparation of the neonatal rat (VF Fill). The preparation is mounted ventral side up (in this example) in an experimental bath on the stage of a fluorescent microscope. Calcium transients produced in fluorescently labeled sacral VFNs are imaged using the attached 14-bit CCD camera, together with the motor output recorded from the L2 and S2 ventral roots during the METH rhythm (Etlin et al., 2013). ***A2***, Electrophysiological recordings from the left and right L2 and S2 ventral root during the development of the METH rhythm (50 μM) are superimposed with 20 s square pulses that denote the opening times of the shutter of the CCD camera during consecutive imaging sessions. The dashed blue line denotes the prerhythm time during which the 10-frame average of the reference image (F) was sampled. This reference image was used to calculate the fluorescence changes ($\Delta F/F$) produced by calcium transients resulting from firing of the imaged cell in the presence of METH (***A4***). ***A3***, The maximal difference image (see Materials and Methods) of an imaged VF neuron in the left S1 segment, sampled during the METH rhythm, is shown encircled by 10 regions of interest used for correction of out-of-focus fluorescence (Etlin et al., 2013). The left VF neuron was back-filled from cut VF axons at the right lumbosacral junction. ***A4***, The calculated $\Delta F/F$ of the labeled crossed projecting VF neuron presented in ***A3***, during the epoch denoted by the green-shaded area in ***A2***, is shown as a function of time, together with the concurrent ventral root recordings of L2 and S2. Note that labeling through cut axons of the right VF, blocked the METH-induced discharge of the right L2 ventral root and that the imaged VF neuron fired in phase with the left S2 and left L2 ventral roots. ***B***, Imaging from a sacral VFN with uncrossed lumbar projections. ***B1***, Electrophysiological recordings from the left (L) and right (R) L2 and S2 ventral roots during the development of the METH rhythm (50 μM) are superimposed on 15 s square pulses denoting the opening time of the shutter of the CCD camera during consecutive imaging sessions. ***B2***, The maximal difference image (see Materials and Methods) of an imaged VFN in the left S1 segment, sampled during the METH rhythm, back-filled from cut VF axons at the left lumbosacral junction. ***B3***, The calculated $\Delta F/F$ of the labeled uncrossed projecting VFN presented in ***B2***, during the epoch denoted by transparent green shading in ***B1***, is shown as a function of time, together with the concurrent ventral root recordings of L2 and S2. Note that labeling through cut axons of the right VF in this case nearly blocked the METH-induced discharge of the right L2 ventral root. Therefore, in this and in similar cases we correlated the signal of the imaged VF cell with the right S2 ventral root. This could be done since the lumbar and sacral bursts produced on a given side of the cord, evoked either by SCA stimulation (Blivis et al., 2007; Strauss and Lev-Tov, 2003; Etlin et al., 2010, 2013) or by METH (Gabbay and Lev-Tov, 2004; Cherniak et al., 2014, the present study) were always in phase with each other.

cut VF at the right lumbosacral junction (Fig. 7*B2*, maximal difference image), this right sacral VF neuron displayed rhythmic calcium transients in the presence of METH (Fig. 7*B3*, VF uncrossed, ΔF/F). Like that of the crossed projecting VF neuron shown in Fig. 7*A*, the activity of this uncrossed projecting VF neuron was in phase with the motor output ipsilateral to its cell body (right S2 and L2; Fig. 7*B3*). The phase to the larger S2 signal in this case was 19.4 ± 3.2°, r-vector = 0.99.

Additional examples of combined optical and electrophysiological recordings in two different experiments appear in Figure 8. The first experiment (Fig. 8*A*) shows how the METH rhythm, recorded from L2 and S2 ventral roots (Fig. 8*A1*) and imaged from three different left VFNs with crossed lumbar projections (Fig. 8*A2*, VF#1–VF#3), develops and stabilizes in the presence of METH during two consecutive 15 s shutter openings (Fig. 8*A1*,*A3*, I, II). The discharge of these cells at the beginning of the recordings (I) was rather irregular. Coherent crossed power (see Materials and Methods) appeared only in 21, 10, and 62% of the spectra, respectively. The discharge of the three VFNs strengthened during the second shutter opening (II), and developed more intensive and robust rhythmic bursting, as the sacral and the concomitant lumbar rhythm strengthened. Like the cells shown in Figure 7, the three crossed projecting VFNs in Figure 8*A3* (shutter opening II) fired in phase with the ventral root discharge ipsilateral to their cell bodies (VF#1: 357.3 ± 6.6°, r-vector = 0.993; VF#2: 358 ± 7.7°, r-vector = 0.991; VF#3: 284.6 ± 2.9°, r-vector = 0.999). The second experiment shown in Figure 8*B1–B3* demonstrates different phase preference of two cross projecting VFNs imaged during the METH rhythm from the left S1/S2 segment (back-filled from the right VF at the lumbosacral junction; Fig. 8*B2*), with the concurrent motor output. In this example, one left VF neuron (VF#1) fired with the left (ipsilateral) S2 and L2 bursting (phase VF#1 vs LL2: 44.24 ± 4.3°, r-vector = 0.997), while the other left S1/S2 VF neuron fired with the right (contralateral) ventral root discharge of S2 and L2 (Fig. 8B3; VF#2 vs RL2: 354.1 ± 3.6°, r-vector = 0.998). Accordingly, the phase between the optic signals of two imaged cells (VF#1 vs VF#2) was 169.8 ± 2.2°, r-vector = 0.999.

To summarize, we performed 16 fluorescence calcium imaging experiments with concurrent recordings of the motor output. Of 203 imaged VFNs with crossed lumbar projections, 80 (39.4%) responded to bath-applied METH. Cross-WT and cross-coherent power analyses of the correlation between VF neuron calcium transients and rostral lumbar motoneuron population discharge revealed that 55 (69%) of the responding VFN with crossed projections (Figs. 7*A*, 8*A*,*B*, VF#1), and all (three neurons) of the responding VFNs with uncrossed projections (Fig. 7*B*), fired with the motor output ipsilateral to their cell bodies. Thirty-one percent of the responding VFNs with crossed projections (25 neurons) fired with the motor output contralateral to their cell bodies (Fig. 8*B*, VF#2). These data are summarized in Figure 8*C*, which shows an illustration of the METH responders and mean phase of their fluorescent changes with the ipsilateral or contralateral motor output.

As mentioned above, our earlier studies had revealed that sacral relay neurons that project rostrally through the VF play an important role in mediation of the locomotor rhythm produced by stimulation of SCAs (Etlin et al., 2010, 2013, 2014; Finkel et al., 2014). Since some of these VFNs are located within the deep ventral aspect of the gray matter, where most of the METH-activated VFNs we imaged in the present study reside, it was of interest to establish whether SCA input can also activate the METH responders to produce rhythmic bursts in rostral lumbar motoneurons. In 11 VFNs, imaged in six experiments, we recorded the responses of the same VFNs to both SCA stimulation and to METH, and tested the correlation between the optical and electrophysiological signals under these conditions. Figure 9*A–C* displays calcium imaging from five different VFNs and concurrent electrophysiological recordings of the motor output in two of six different experiments. Three of these five neurons responded to both SCA stimulation and METH application (Fig. 9, VF#1, VF#2, and VF#5; compare left SCA with right METH). The phase preference of these three SCA+METH responders during SCA stimulation did not change in the presence of METH. The respective mean phase values were as follows: VF#1 versus LS2 phase: SCA, 2.9 ± 3°, r-vector = 0.99; METH, 8.5 ± 5.5°, r-vector = 0.99; VF#2 versus RS2 phase: SCA, 12.8 ± 4.9°, r-vector = 0.99; METH, 9.5 ± 2.5°, r-vector = 0.99; VF#5 versus RS2 phase: SCA, 17.6 ± 3.7°, r-vector = 0.99; METH, 14.2 ± 3.6°, r-vector = 0.99. One of the five imaged neurons responded only to METH (Fig. 9*B*, VF#3 METH; VF#3 versus RS2: METH, 12.85 ± 4.9°, r-vector = 0.99) but not to SCA stimulation (Fig. 9*B*, VF#3 SCA). Another VF neuron responded only to SCA stimulation (Fig. 9*C*, VF#4 SCA; VF#4 versus RS2: SCA, 13.9 ± 7°, r-vector = 0.99) but not to METH (Fig. 9*C*, VF#4 METH). Altogether, it appears that the heterogeneous population of sacral relay neurons with ascending lumbar projections through the VF provides adequate and versatile means to affect the performance of rostral lumbar motoneurons and rhythmogenic circuitry during specific motor behaviors, as discussed below.

Discussion

METH activates long-projecting, ventral–sacral VFNs to produce the "fast" lumbar rhythm

Activated adrenoceptors modulate locomotor rhythms produced in newborn and adult mammals and shape the output of lumbar motoneurons (Rossignol et al., 1996; Barbeau and Norman, 2003; Miles and Sillar, 2011; Rank et al., 2011; Cherniak et al., 2014). The present study is concerned with identifying the pathways that link SCPGs to rostral-lumbar motoneurons, thereby enabling METH-activated SCPGs to modulate and shape the lumbar motor output and increase the capacity of stimulated lumbar afferents to produce locomotor-like rhythm (Fig. 2*A*).

Altogether, our findings suggest that the METH-activated SCPGs reside within the gray matter ventrally to the central canal, that sacral VFNs with lumbar projections transmit the drive required for initiation of fast METH-bursting in lumbar flexors, and that METH-activated VFNs connect directly to rostral lumbar segments. We found that METH-responding VFNs fired rhythmically, in phase with the concurrent ipsilateral or contralateral motor output. Some of the METH-responding VFNs also fired during SCA stimulation. The contribution of ascending sacral projections to activation and modulation of lumbar circuitry are discussed, aided by a simple connectivity model.

Sacral initiation and modulation of lumbar motor activity

Heterogeneous populations of sacral neurons mediate the rhythms induced by SCA stimulation and bath-applied METH. Sacral neurons projecting through the VLF, LF, DLF, and VF mediate the SCA-induced locomotor rhythm (Etlin et al., 2010, 2013), while the fast lumbar METH rhythm depends on activation of the SCPGs and is mediated exclusively by long-projecting VFNs to rostral lumbar segments. Accordingly, this fast rhythm is blocked when the VF is interrupted at the sacral (Fig. 6*A*) or midlumbar level (Fig. 6*C*), and is maintained following synaptic block between caudal-L6 and caudal-L2 (Fig. 6*C*). In contrast,

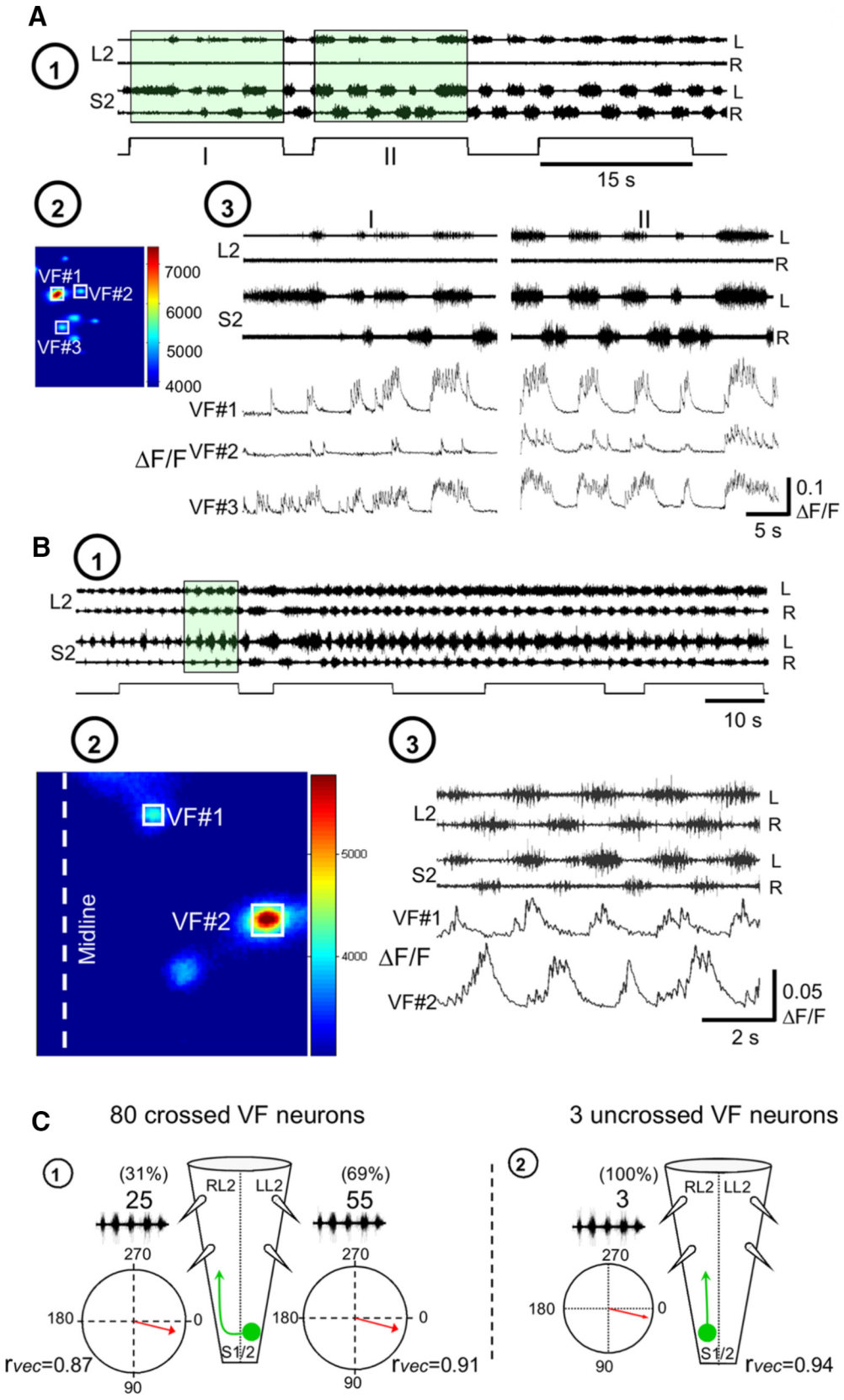

Figure 8. Development of the METH rhythm in sacral VFNs and its phase preference. ***A***, Stabilization of METH-induced rhythmic discharge in VFNs. ***A1***, AC recordings (20 Hz to 10 kHz) from the left (L) and right (R) ventral roots of S2 and L2 during rhythmic activity produced by bath application of 50 μM METH in P1 pups. Fluorescent imaging during the first two exposures to fluorescence excitation (I and II; 15 s each) are denoted by square pulses in green-shaded areas. ***A2***, The mean reference image (see Materials and Methods) of three imaged VFNs (VF#1, VF#2, and VF#3) in the left S1 segment, sampled before the METH rhythm, back-filled from cut VF axons at the left lumbosacral junction. ***A3***, The activity (ΔF/F) of three L-S2 VFNs (VF#1, VF#2, and VF#3) back-labeled from cut VF axons at the right L6/S1 junction, and the concurrently recorded motor output shown during two consecutive fluorescence excitations (***A1***). Note the enhancement and stabilization of the rhythmic discharge of the three cells, and the concurrent motor output in the second exposure. The phase locking of the discharge of the three neurons (*Figure legend continues.*)

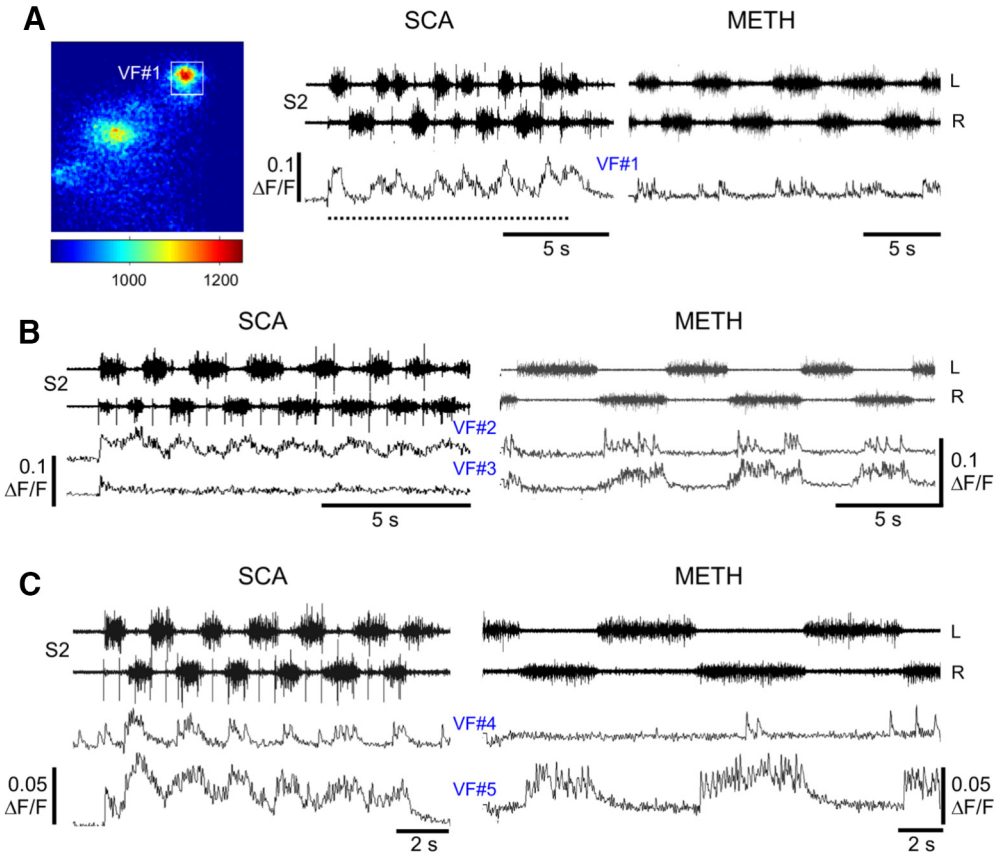

Figure 9. Some VFNs respond to METH and SCA stimulation, while others respond only to METH or only to SCA stimulation. ***A***, The activity (ΔF/F) of a left S1/2 VFN (difference image on left) back-filled from the right VF (at L6/S1) and the concurrent motor output (20 Hz to 10 kHz S2 recordings) during SCA stimulation and in the presence of 100 μM METH. The neuron (VF#1) discharged rhythmically in both cases, in phase with the motor output ipsilateral to its cell body (see text). ***B***, The activity (ΔF/F) of two left S1/2 VFN (VF#2 and VF#3) back-filled from the right L6/S1 VF, together with the concurrent motor output during SCA stimulation and in the presence of METH. Neuron VF#2 discharged rhythmically in response to SCA and to 100 μM METH, in phase with the motor output contralateral to its cell body. Neuron VF#3 fired rhythmically only in the presence of METH. The discharge was in phase with the motor output contralateral to its cell body (see text). ***C***, The activity (ΔF/F) of two different left S1/2 VFNs (VF#4 and VF#5) back-filled from the right VF (at L6/S1) and the concurrent motor output during SCA stimulation or in the presence of METH, in the same experiment as shown in ***B***. Neuron VF#4 discharged rhythmically in response to SCA, in phase with the motor output contralateral to its cell body, but did not respond to METH. Neuron VF#5 fired rhythmically in response to SCA and METH, in phase with the motor output contralateral to its cell body (see text). All electrophysiological data were recorded at AC 20 Hz to 10 kHz. The parameters of the SCA stimulations were 20 pulse, 1.66 Hz, at 20 μA in ***A***, and 22 μA in ***B*** and ***C***. All wavelet-based correlation analyses of the data shown in ***A–C*** were done using the imaged VFNs and the respective S2 discharge (as in Fig. 7*B*).

the VF-dependent component of the SCA-induced locomotor rhythm does not necessarily require activation of the SCPGs (Etlin et al., 2013). Furthermore, it is mediated by long-projecting sacral VFNs and also by short-projecting sacral VFNs that serially recruit sacral (Etlin et al., 2010) and lumbar (M. Cherniak and A. Lev-Tov, unpublished data) propriospinal neurons that activate the LCPGs. This serial recruitment enables the VF-dependent component of the SCA-induced locomotor rhythm to survive interruptions of sacral and lumbar VF, and its absence during caudal-L6 to caudal-L2 synaptic block leads to a substantial decrease in power of the lumbar motor output (Etlin et al., 2010).

There are also some similarities between the METH-activated and SCA-activated pathways. Our calcium-imaging studies revealed of that some of the METH-responding sacral VFNs responded also to SCA stimulation, while others responded only to METH or SCA stimulation (Fig. 9). Because all METH responders project directly to rostral lumbar motoneurons exclusively through the VF (Fig. 6), those VFNs that respond to both METH and SCA should also project to rostral lumbar motoneurons and modulate their output during noradrenergic and sacral afferent activation of the SCPGs (Fig. 10).

Thus, the projections of SCA-activated sacral VFNs to the LCPGs allow sacral networks to activate the LCPGs and modulate their frequency. At the same time, the direct projections of the METH and METH/SCA-activated VFNs to rostral lumbar motoneurons enable the sacral networks to shape the motor output of lumbar flexors, in accord with the functional requirements at a

←

(*Figure legend continued.*) to the motor output ipsilateral to their cell bodies (left S2 and L2) should also be noted. ***B***, Different phase preferences of METH-activated sacral VFNs. ***B1***, AC recordings (20 Hz to 10 kHz) from the left (L) and right (R) ventral roots of S2 and L2, during rhythmic activity produced by bath application of 50 μM METH, are superimposed with the shutter openings of the digital CCD camera used for imaging (square pulses). ***B2***, Maximal difference images of left S1 cross-projecting VFNs (left), during exposure to METH. The neurons VF#1 and VF#2 were labeled with Calcium Green dextran through cut VF axons at the right lumbosacral junction in P1 pups. ***B3***, The activity (ΔF/F) of two L-S1 VFNs (VF#1 and VF#2) shown as a function of time with the concurrent L2 and S2 recordings. The green-shaded area in ***B1*** denotes the sampling epoch of the recorded data. Note the different phase preferences of the two imaged VFNs. ***C***, Illustrated summary of the phase preferences of METH-responding VFNs with crossed projections (***C1***) and uncrossed projections (***C2***). The circular plots show the phase with the motor output either ipsilateral or contralateral to the somata of the labeled VFNs. r_{vec}, Respective r-vector values. Our back-labeling experiments of sacral relay neurons through the cut VF at the lumbosacral junction revealed that 93% of the VFNs (Fig. 3 legend) and 92% in research by Etlin et al. (2010) had crossed lumbar projections. In the present study, we back-filled and imaged 201 VFNs with crossed lumbar projections. Eighty of them (40%) responded to METH. In two of the experiments, we imaged five VF sacral neurons with uncrossed projections, three of which responded to METH.

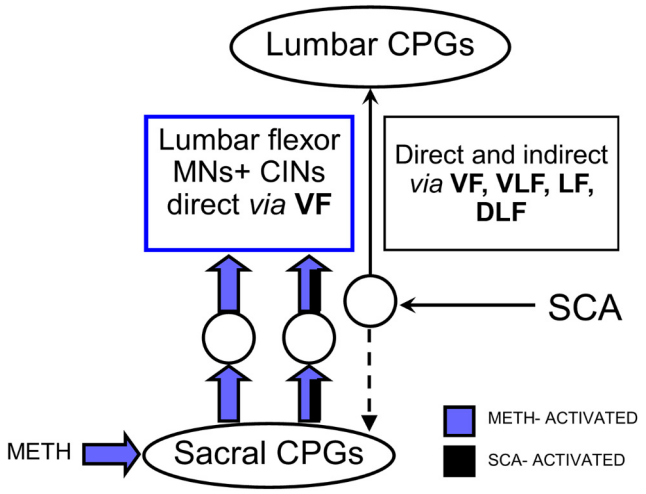

Figure 10. Differential projections of populations of sacral VFNs to the LCPGs and to lumbar flexor motoneurons. SCA stimulation activates the sacral and the LCPGs. The drive produced by SCA stimulation, in crossed and uncrossed, direct and indirect projecting sacral relay neurons, ascends to the LCPGs through the VF, VLF, LF, and DLF (right, thin black arrows). In the presence of METH (blue), the sacral CPGs activate two populations of relay neurons with direct crossed and uncrossed projections traveling only through the VF to lumbar flexor motoneurons and to rostral lumbar commissural interneurons. The first population discharges only when the sacral CPGs are activated by METH (left, blue filled arrows), the second one fires when the sacral CPGs are activated by either METH or SCA stimulation (middle, blue and black filled arrows). The diverse effects of sacral networks on the frequency and motor output of the LCPGs, described by Etlin et al. (2013) and Finkel et al. (2014), also reflect this differential connectivity to motoneurons and to the locomotor CPGs. Possible activation of motoneurons by SCA stimulation not via the sacral CPGs (Strauss and Lev-Tov, 2003; Etlin et al., 2013) is not shown in this scheme.

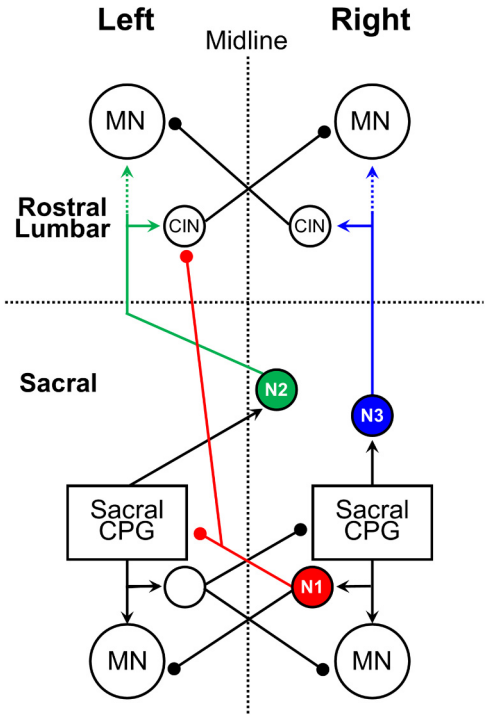

Figure 11. A suggested model for sacrolumbar connectivity that can account for the sacrally induced lumbar METH rhythm. The model presented suggests that three classes of sacral VFNs (N1–N3), activated by the sacral CPGs in the presence of METH (Figs. 7, 8*C1*,*C2*, 9), are responsible for the alternating left–right rhythmic bursting in rostral lumbar motoneurons. The three classes of neurons (whose cell bodies, for simplicity, are shown only for the right hemicord) are as follows: Neuron 1 (N1, red), inhibitory, is activated by the adjacent ipsilateral SCPGs. It fires with the ipsilateral motor output (both sacral and lumbar; Fig. 8*C1*) and it projects to the contralateral ICINs at the rostral lumbar cord (see Discussion). Neuron 2 (N2, green), excitatory, fires with the contralateral motor output (Fig. 8*C1*), is activated by the contralateral SCPGs, and projects to the contralateral rostral lumbar motoneurons and rostral lumbar ICINs (see Discussion). Neuron 3 (N3, blue), excitatory, fires with the ipsilateral motor output (Fig. 8*C2*), is activated by the adjacent ipsilateral sacral CPGs, and sends uncrossed projections to rostral lumbar motoneurons and to rostral lumbar inhibitory commissural interneurons (CIN; as in Fig. 7*B*; see Discussion). Arrowheads, Excitatory projections; filled circles, inhibitory projections; MN, motoneuron. Dashed arrows of N2 and N3 denote mono/oligosynaptic connectivity through the L6-L3 segments. Note that the ipsilateral sacral CPGs drive the ipsilateral N1s and N3s (shown in the scheme) and the contralateral N2s (left, data not shown in the scheme), and that all three of them increase the excitability of the ipsilateral motor output of L2 (for further details, see text).

given moment. We also showed that sacral METH facilitated the motor output produced during locomotor-like rhythm elicited by lumbar afferent stimulation. Mentis et al. (2005; reviewed by O'Donovan et al., 2010) have shown that ventral root stimulation activated recurrent excitatory pathways (Machacek and Hochman, 2006) between stimulated motor axons and LCPGs and thereby produced locomotor rhythm in the mouse cord. We suggest that by a similar mechanism, the flexor motoneuron firing induced by sacral METH increased the excitability of the LCPGs and thereby enabled the low-intensity lumbar afferent stimulation to exceed threshold and produce locomotor-like rhythm.

The firing pattern of sacral relay neurons and its correlation to the motor output

Our calcium imaging studies (Figs. 7–9) showed that the METH-responding VFNs fired rhythmically only upon activation of the SCPGs. In contrast, SCA-activated sacral VFNs had either rhythmic or nonrhythmic discharge, and the resultant locomotor rhythm did not depend on activation of the SCPGs and the rhythmic VFNs, although the motor output strengthened significantly during their activity (Etlin et al., 2013).

Correlation analysis of VFNs firing and the concurrent motor output offers further insights into sacrolumbar coupling during the METH rhythm. Most sacral VFNs (93%; Etlin et al., 2010, 2013; Fig. 3*B*) have crossed lumbar projections. Figure 8*C* shows that 70% of the crossed projecting METH responders fired with the ipsilateral motor output and 30% fired with the contralateral motor output. It is reasonable to assume that crossed projecting VFNs that fire with the ipsilateral motor output (Figs. 7*A*, 8*A*,*C*) are inhibitory; crossed projecting VFNs firing with the contralateral motor output (Figs. 8*B*, #VF2, 9*B*, #VF2, #VF3, #VF5) are excitatory; neurons with uncrossed projections that fire with the ipsilateral motor (Fig. 7*B*) are also excitatory. We termed these three groups of neurons N1, N2. and N3, respectively. The proportion of our assumed inhibitory–excitatory crossed projecting METH responders (N1/N2) are comparable to proportions of inhibitory commissural neurons (ICINs; 70%) and excitatory commissural neurons (30%) in the rodent lumbar cord (Lanuza et al., 2004). In Figure 11 we propose a model of the sacrolumbar connectivity suggesting how METH-activated SCPGs can shape the output of rostral lumbar motoneurons. For simplicity, we show the somata of N1–N3 neurons only for the right hemicord.

N1s are inhibitory crossed projecting sacral VFNs. Because the crossed inhibition between lumbar flexors disappeared following midsagittal lumbar split, while left–right alternation persisted (Gabbay and Lev-Tov, 2004), we suggest that N1s project to contralateral lumbar ICINs. Consequently, N1s disinhibit flexors ipsilateral to their somata, thereby increasing their discharge.

N2s are excitatory crossed projecting sacral VFNs. Because the METH-induced sacral and lumbar discharge on a given side of the cord are always in phase, we suggest that N2s are activated by the contralateral SCPGs through a crossed excitatory link. When

activated by the contralateral SCPGs, N2s excite contralateral lumbar flexor motoneurons and inhibit motoneurons ipsilateral to their somata via lumbar ICINs.

N3s are excitatory VFNs with uncrossed projections to lumbar commissural interneurons and motoneurons. When activated by the ipsilateral SCPGs, N3s excite ipsilateral lumbar flexor motoneurons and inhibit contralateral flexor motoneurons through lumbar ICINs.

This model explains the connectivity used to produce the fast lumbar bursting produced by METH-activated SCPGs. It also clarifies how the alternating phasic excitation provided by crossed (N2) and uncrossed projections (N3) of the excitatory VFNs driven by the ipsilateral and contralateral SCPGs can maintain the left–right alternating bursts of lumbar flexors reported in midsagitally split lumbar cord, after removal of crossed inhibition (Gabbay and Lev-Tov, 2004).

Our model assumes mono/oligo synaptic connectivity between sacral VFNs and rostral lumbar circuitry based on our findings as follow: (1) interruption of VF at the lumbosacral junction (Fig. 6*A*,*B*) and at any point along the L6-caudal L2 (Fig. 6*C*) blocked METH-induced L2 firing; (2) sacral METH-induced L2 firing changed only slightly when synaptic transmission along caudal-L6 to caudal-L2 was blocked (Fig. 6*D*); (3) stimulation of cut L6/S1 VF axons produced VRPs with monosynaptic-like latencies (Fig. 6*E*); and (4) viral-vector trans-synaptic labeling of premotoneurons is feasible in the rodent cord (Stepien et al., 2010; Arber, 2012). Using injection of pseudorabies virus coupled to GFP (PRV.GFP; Jovanovic et al., 2010) to hindlimb muscles, our preliminary experiments revealed ipsilateral and contralateral labeled PRV.GFP interneurons in S1/S2 with VF, VLF and LF labeled axons 40–48 h following the injection (Roisman et al., 2014). Most recently, we showed further that Texas red dextran back-filled sacral VFNs colabeled some previously labeled PRV.GFP premotoneurons ~40 h following PRV.GFP injection to hindlimb muscles (M. Cherniak, E. Hassidov, A. Lev-Tov, unpublished data).

It should be noted that the suggested mono/oligosynaptic connectivity may include long projections of excitatory VFNs onto rostral lumbar V0c neurons, a group of cholinergic neurons adjacent to the central canal that contact spinal motoneurons through c-boutons and modulate the motoneuron excitability (Miles et al., 2007; Zagoraiou et al., 2009; Stepien et al., 2010).

Conclusions

Rhythmic activity produced by the SCPGs activates the tail and regional axial musculature to stabilize the body during various motor behaviors. The METH-activated SCPGs have the capacity to excite lumbar flexor motoneurons to fire "fast" rhythmic bursts, thereby providing sacral networks with a potent means to control the output of lumbar motoneurons and affect the behavior produced by the LCPGs. We identified the mediating sacral VFNs and the ascending circuitry interposed between the SCPGs and lumbar networks. Although the model we presented above is plausible, further studies are required to provide information about the excitatory/inhibitory nature of the relay neurons, and the trajectories of their ascending projection to lumbar motoneurons. We are currently pursuing these issues in series of rodent experiments exploiting methods adapted from Hadas et al. (2014). Additional emphasis should be given to further clarification of whether and how our findings can be implemented to adult mammals, in line with the reported significance of adrenoceptor-mediated effects on the spinal cord, specifically after injury and disruption of supraspinal control.

References

Alford S, Schwartz E, Viana di Prisco G (2003) The pharmacology of vertebrate spinal central pattern generators. Neuroscientist 9, 217–28. CrossRef Medline

Arber S (2012) Motor circuits in action: specification, connectivity, and function. Neuron 74:975–989. CrossRef Medline

Barbeau H, Norman KE (2003) The effect of noradrenergic drugs on the recovery of walking after spinal cord injury. Spinal Cord 41:137–143. CrossRef Medline

Blivis D, Mentis GZ, O'Donovan MJ, Lev-Tov A (2007) Differential effects of opioids on sacrocaudal afferent pathways and central pattern generators in the neonatal rat spinal cord. J Neurophysiol 97:2875–2886. CrossRef Medline

Bonnot A, Whelan PJ, Mentis GZ, O'Donovan MJ (2002) Spatiotemporal pattern of motoneuron activation in the rostral lumbar and the sacral segments during locomotor-like activity in the neonatal mouse spinal cord. J Neurosci 22:RC203. Medline

Bonnot A, Mentis GZ, Skoch J, O'Donovan MJ (2005) Electroporation loading of calcium-sensitive dyes into the CNS. J Neurophysiol 93:1793–1808. Medline

Cazalets JR, Bertrand S (2000) Coupling between lumbar and sacral motor networks in the neonatal rat spinal cord. Eur J Neurosci 12:2993–3002. CrossRef Medline

Cherniak M, Etlin A, Strauss I, Anglister L, Lev-Tov A (2014) The sacral networks and neural pathways used to elicit lumbar motor rhythm in the rodent spinal cord. Front Neural Circuits 8:143. CrossRef Medline

Delvolvé I, Gabbay H, Lev-Tov A (2001) The motor output and behavior produced by rhythmogenic sacrocaudal networks in spinal cords of neonatal rats. J Neurophysiol 85: 2100–2110. Medline

Dietz V, Müller R, Colombo G (2002) Locomotor activity in spinal man: significance of afferent input from joint and load receptors. Brain 125: 2626–2634. CrossRef Medline

Dose F, Deumens R, Forget P, Taccola G (2016) Staggered multi-site low-frequency electrostimulation effectively induces locomotor patterns in the isolated rat spinal cord. Spinal Cord 54:93–101. CrossRef Medline

Edgerton VR, Courtine G, Gerasimenko YP, Lavrov I, Ichiyama RM, Fong AJ, Cai LL, Otoshi CK, Tillakaratne NJ, Burdick JW, Roy RR (2008) Training locomotor networks. Brain Res Rev 57:241–254. CrossRef Medline

Etlin A, Blivis D, Ben-Zwi M, Lev-Tov A (2010) Long and short multifunicular projections of sacral neurons are activated by sensory input to produce locomotor activity in the absence of supraspinal control. J Neurosci 30:10324–10336. CrossRef Medline

Etlin A, Finkel E, Mor Y, O'Donovan MJ, Anglister L, Lev-Tov A (2013) Characterization of sacral interneurons that mediate activation of locomotor pattern generators by sacrocaudal afferent input. J Neurosci 33: 734–747. CrossRef Medline

Etlin A, Finkel E, Cherniak M, Lev-Tov A, Anglister L (2014) The motor output of hindlimb innervating segments of the spinal cord is modulated by cholinergic activation of rostrally projecting sacral relay neurons. J Mol Neurosci 53:517–524. CrossRef Medline

Finkel E, Etlin A, Cherniak M, Mor Y, Lev-Tov A, Anglister L (2014) Neuroanatomical basis for cholinergic modulation of locomotor networks by sacral relay neurons with ascending lumbar projections. J Comp Neurol 522:3437–3455. CrossRef Medline

Floeter MK, Lev-Tov A (1993) Excitation of lumbar motoneurons by the medial longitudinal fasciculus in the neonatal rat brainstem spinal cord preparation. J Neurophysiol 70:2241–2250. Medline

Frigon A (2012) Central pattern generators of the mammalian spinal cord. Neuroscientist 18:56–69. CrossRef Medline

Gabbay H, Lev-Tov A (2004) Alpha-1 adrenoceptor agonists generate a "fast" NMDA receptor-independent motor rhythm in the neonatal rat spinal cord. J Neurophysiol 92:997–1010. CrossRef Medline

Gabbay H, DelvolvéI, Lev-Tov A (2002) Pattern generation in caudal-lumbar and sacrococcygeal segments of the neonatal rat spinal cord. J Neurophysiol 88:732–739. Medline

Gordon IT, Whelan PJ (2006) Monoaminergic control of cauda-equina-evoked locomotion in the neonatal mouse spinal cord. J Neurophysiol 96:3122–3129. CrossRef Medline

Grillner S, Rossignol S (1978) On the initiation of the swing phase of locomotion in chronic spinal cats. Brain Res 146:269–277. CrossRef Medline

Grillner S, Zangger P (1979) On the central generation of locomotion in the low spinal cat. Exp Brain Res 34:241–261. Medline

Hadas Y, Etlin A, Falk H, Avraham O, Kobiler O, Panet A, Lev-Tov A, Klar A (2014) A 'tool box' for deciphering neuronal circuits in the developing chick spinal cord. Nucleic Acids Res 42:e148. CrossRef Medline

Hubli M, Dietz V (2013) The physiological basis of neurorehabilitation—locomotor training after spinal cord injury. J Neuroeng Rehabil 10:5. CrossRef Medline

Hultborn H, Nielsen JB (2007) Spinal control of locomotion—from cat to man. Acta Physiol (Oxf) 189:111–121. CrossRef Medline

Jovanovic K, Pastor AM, O'Donovan MJ (2010) The use of PRV-Bartha to define premotor inputs to lumbar motoneurons in the neonatal spinal cord of the mouse. PloS One 5:e11743. CrossRef Medline

Kasumacic N, Glover JC, Perreault MC (2010) Segmental patterns of vestibular-mediated synaptic inputs to axial and limb motoneurons in the neonatal mouse assessed by optical recording. J Physiol 588:4905–4925. CrossRef Medline

Kiehn O (2006) Locomotor circuits in the mammalian spinal cord. Annu Rev Neurosci 29:279–306. CrossRef Medline

Kiehn O, Sillar KT, Kjaerulff O, McDearmid JR (1999) Effects of noradrenaline on locomotor rhythm-generating networks in the isolated neonatal rat spinal cord. J Neurophysiol 82:741–746. Medline

Klein DA, Tresch MC (2010) Specificity of intramuscular activation during rhythms produced by spinal patterning systems in the in vitro neonatal rat with hindlimb attached preparation. J Neurophysiol 104:2158–2168. CrossRef Medline

Kremer E, Lev-Tov A (1997) Localization of the spinal network associated with generation of hindlimb locomotion in the neonatal rat and organization of its transverse coupling system. J Neurophysiol 77:1155–1170. Medline

Kudo N, Yamada T (1987) N-methyl-D, L-aspartate-induced locomotor activity in a spinal cord-hindlimb muscles preparation of the newborn rat studied in vitro. Neurosci Lett 75:43–48. CrossRef Medline

Lanuza GM, Gosgnach S, Pierani A, Jessell TM, Goulding M (2004) Genetic identification of spinal interneurons that coordinate left-right locomotor activity necessary for walking movements. Neuron 42:375–386. CrossRef Medline

Leblond H, L'Esperance M, Orsal D, Rossignol S (2003) Treadmill locomotion in the intact and spinal mouse. J Neurosci 23:11411–11419. Medline

Lev-Tov A, Delvolvé I (2000) Pattern generation in non-limb moving segments of the mammalian spinal cord. Brain Res Bull 53:671–675. Medline

Lev-Tov A, O'Donovan MJ (1995) Calcium imaging of motoneuron activity in the en-bloc spinal cord preparation of the neonatal rat. J Neurophysiol 74:1324–1334. Medline

Lev-Tov A, Delvolvé I, Kremer E (2000) Sacrocaudal afferents induce rhythmic efferent bursting in isolated spinal cords of neonatal rats. J Neurophysiol 83:888–894. Medline

Lev-Tov A, Etlin A, Blivis D (2010) Sensory-induced activation of pattern generators in the absence of supraspinal control. Ann NY Acad Sci 1198:54–62. CrossRef Medline

Machacek DW, Hochman S (2006) Noradrenaline unmasks novel self-reinforcing motor circuits within the mammalian spinal cord. J Neurosci 26:5920–5928. CrossRef Medline

Majczyński H, Sławińska U (2007) Locomotor recovery after thoracic spinal cord lesions in cats, rats and humans. Acta Neurobiol Exp (Wars) 67:235–257. Medline

Mandadi S, Whelan PJ (2009) A new method to study sensory modulation of locomotor networks by activation of thermosensitive cutaneous afferents using a hindlimb attached spinal cord preparation. J Neurosci Methods 182:255–259. CrossRef Medline

Marchetti C, Beato M, Nistri A (2001) Alternating rhythmic activity induced by dorsal root stimulation in the neonatal rat spinal cord in vitro. J Physiol 530:105–12. CrossRef Medline

Mentis GZ, Alvarez FJ, Bonnot A, Richards DS, Gonzalez-Forero D, Zerda R, O'Donovan MJ (2005) Non-cholinergic excitatory actions of motoneurons in the neonatal mammalian spinal cord. Proc Natl Acad Sci U S A 102:7344–7349. CrossRef Medline

Miles GB, Sillar KT (2011) Neuromodulation of vertebrate locomotor control networks. Physiology 26:393–411. CrossRef Medline

Miles GB, Hartley R, Todd AJ, Brownstone RM (2007) Spinal cholinergic interneurons regulate the excitability of motoneurons during locomotion. Proc Natl Acad Sci U S A 104:2448–2453. CrossRef Medline

Mor Y, Lev-Tov A (2007) Analysis of rhythmic patterns produced by spinal neural networks. J Neurophysiol 98:2807–2817. CrossRef Medline

Mor Y, Etlin A, Shamir B, Zeilig G, Lev-Tov A (2012a) Graphic processing unit (GPU)-based wavelet analysis of the rhythmic output produced by spinal pattern generators. J Mol Neurosci 48 [Suppl 1]:S81.

Mor Y, Etlin A, Shamir B, Zeilig G, Lev-Tov A (2012b) Wavelet analysis of linear and non-linear interactions between constituents of rhythmic motor output is made possible by graphic processing unit (GPU)-based parallel computing. J Mol Neurosci 48 [Suppl 1]:1. CrossRef

O'Donovan MJ, Ho S, Sholomenko G, Yee W (1993) Real-time imaging of neurons retrogradely and anterogradely labelled with calcium-sensitive dyes. J Neurosci Methods 46:91–106. CrossRef Medline

O'Donovan M, Ho S, Yee W (1994) Calcium imaging of rhythmic network activity in the developing spinal cord of the chick embryo. J Neurosci 14:6354–6369. Medline

O'Donovan MJ, Bonnot A, Mentis GZ, Chub N, Pujala A, Alvarez FJ (2010) Mechanisms of excitation of spinal networks by stimulation of the ventral roots. Ann N Y Acad Sci 1198:63–71. Medline

Pearson KG (2004) Generating the walking gait: role of sensory feedback. Prog Brain Res 143:123–129. CrossRef

Pearson KG, Rossignol S (1991) Fictive motor patterns in chronic spinal cats. J Neurophysiol 66:1874–1887. Medline

Pinco M, Lev-Tov A (1994) Synaptic transmission between ventrolateral funiculus axons and lumbar motoneurons in the isolated spinal cord of the neonatal rat. J Neurophysiol 72:2406–2419. Medline

Rank MM, Murray KC, Stephens MJ, D'Amico J, Gorassini MA, Bennett DJ (2011) Adrenergic receptors modulate motoneuron excitability, sensory synaptic transmission and muscle spasms after chronic spinal cord injury. J Neurophysiol 105:410–422. CrossRef Medline

Roisman R, Cherniak M, Lev-Tov A (2014) Caudo-rostral coupling between alpha-1 adrenoceptor activated cluster of sacral interneurons and rostral lumbar motoneurons. J Mol Neurosci 53[Suppl 1]:S107–S108.

Rossignol S, Frigon A (2011) Recovery of locomotion after spinal cord injury: some facts and mechanisms. Annu Rev Neurosci 34:413–440. CrossRef Medline

Rossignol S, Chau C, Brustein E, Belanger M, Barbeau H, Drew T (1996) Locomotor capacities after complete and partial lesions of the spinal cord. Acta Neurobiol Exp (Wars) 56:449–463. Medline

Smith JC, Feldman JL, Schmidt BJ (1988) Neural mechanisms generating locomotion studied in mammalian brain stem-spinal cord in vitro. FASEB J 2:2283–2288. Medline

Sqalli-Houssaini Y, Cazalets JR (2000) Noradrenergic control of locomotor networks in the in vitro spinal cord of the neonatal rat. Brain Res 852:100–109. CrossRef Medline

Stepien AE, Tripodi M, Arber S (2010) Monosynaptic rabies virus reveals premotor network organization and synaptic specificity of cholinergic partition cells. Neuron 68:456–472. CrossRef Medline

Strauss I, Lev-Tov A (2003) Neural pathways between sacrocaudal afferents and lumbar pattern generators in neonatal rats. J Neurophysiol 89:773–784. Medline

Taccola G (2011) The locomotor central pattern generator of the rat spinal cord in vitro is optimally activated by noisy dorsal root waveforms. J Neurophysiol 106:872–884. CrossRef Medline

Wernig A, Nanassy A, MüllerS (1998) Maintenance of locomotor abilities following Laufband (treadmill) therapy in para- and tetraplegic persons: follow-up studies. Spinal Cord 36:744–749. CrossRef Medline

Whelan P, Bonnot A, O'Donovan MJ (2000) Properties of rhythmic activity generated by the isolated spinal cord of the neonatal mouse. J Neurophysiol 84:2821–2833. Medline

Zagoraiou L, Akay T, Martin JF, Brownstone RM, Jessell TM, Miles GB (2009) A cluster of cholinergic premotor interneurons modulates mouse locomotor activity. Neuron 64:645–662. CrossRef Medline

Zar J (1999) Biostatistical analysis, 4th edition. Upper Saddle River, NJ: Prentice Hall.